Buffering of atmospheric nanoparticle growth by temperature-dependent shifts in molecular composition, volatility and diffusivity

Zhiqiang Zhang[1], Hyun Gu Kang[1], Ulrich Pöschl[1], and Thomas Berkemeier[1]

[1]Multiphase Chemistry Department, Max Planck Institute for Chemistry, Hahn-Meitner-Weg 1, 55128 Mainz, Germany

Correspondence: Thomas Berkemeier (t.berkemeier@mpic.de)

Abstract

Aerosols have a profound influence on climate and human health, but new particle formation in the atmosphere has remained a scientific conundrum. In particular, the growth rates of atmospheric nanoparticles are often smaller and less dependent on condensable vapor concentration than expected. Here, we take a new integrative approach to analyze observational data from field measurements and chamber experiments, which were previously unexplained and appeared inconsistent with theory and model predictions. We show that the observed growth rates can be predicted when the temperature dependence and multiphase kinetics of gas-particle partitioning are resolved. Slow surface-to-bulk transport limits the rates of vapor uptake by semi-solid particles with low diffusivity, whereas shifts in the volatility distribution following the Clausius-Clapeyron equation enhance growth rates at low temperature and concentration levels. These antagonistic effects lead to an effective buffering of the organic vapor concentration dependence of nanoparticle growth in secondary organic aerosols. Our study reveals how counteracting temperature dependencies of organic vapor oxidation, volatility and diffusivity can explain the convergence of growth rates around a few nanometers per hour under widely varying atmospheric conditions.

1 Introduction

Atmospheric aerosols consisting of airborne particles in the nanometer to micrometer size range have a strong influence on air quality, public health, and climate (IPCC, 2023; WHO, 2023). Large fractions of airborne fine particulate matter consist of secondary organic aerosols (SOA) formed by gas-to-particle conversion of organic precursor molecules in the atmosphere (Jimenez et al., 2009; Hallquist et al., 2009; Riipinen et al., 2011; Shrivastava et al., 2017). Over the past decades, numerous studies have investigated atmospheric new particle formation and growth (Kulmala et al., 2004, 2014; Stolzenburg et al., 2023). The rates of nanoparticle growth, however, have remained enigmatic and constitute a gap in the scientific understanding and assessment of atmospheric aerosols and their effects on health and climate (Bianchi et al., 2016; Gordon et al., 2017; Kulmala et al., 2022). In particular, the growth rates of atmospheric SOA particles observed in field measurements are fairly uniform around 1-10 nm h^{-1} and exhibit a relatively weak dependence on measured organic vapor concentrations that vary by multiple

orders of magnitude (Stolzenburg et al., 2018; Yli-Juuti et al., 2020; Stolzenburg et al., 2025). Computational models utilizing volatility basis sets (VBS; Donahue et al., 2006, 2011; Bhattacharyya et al., 2025) were found to reproduce observations under a variety of conditions, while under- or over-predicting nanoparticle growth rates measured in other instances (Stolzenburg et al., 2018; Mohr et al., 2019; Qiao et al., 2021; Stolzenburg et al., 2022; Dada et al., 2023; Cai et al., 2026).

Under atmospheric conditions, organic aerosol particles are expected to exist in highly viscous or semi-solid phase states and may even exhibit an amorphous solid (glassy) state depending on chemical composition, temperature, and humidity (Zobrist et al., 2008; Mikhailov et al., 2009; Virtanen et al., 2010; Koop et al., 2011; Renbaum-Wolff et al., 2013; Shiraiwa et al., 2017; Reid et al., 2018). Accordingly, the molecular diffusivity in SOA particles can vary over a wide range from more than 10^{-10} cm^2 s^{-1} (liquid) to less than 10^{-21} cm^2 s^{-1} (glassy), which influences the kinetics of mass transport, gas uptake, and partitioning (Shiraiwa et al., 2011; Berkemeier et al., 2013; Shiraiwa et al., 2014; Zaveri et al., 2018; Li et al., 2026). Earlier studies have shown that diffusivity-limitations can affect the water uptake, heterogeneous chemical transformation, evaporation, and size distribution of organic aerosol particles (Pfrang et al., 2011; Zhou et al., 2013; Arangio et al., 2015; Berkemeier et al., 2014, 2016; Mu et al., 2018; Zaveri et al., 2020; Berkemeier et al., 2020; Schervish et al., 2026; Kang et al., 2026).

Here, we re-analyze observational data of nanoparticle growth from field measurements in the boreal forest (Hyytiälä, Finland) and from sophisticated laboratory experiments (CERN CLOUD), utilizing a new kinetic multilayer model of multiphase chemistry (KM3C) that resolves the reactivity, diffusivity, and concentration gradients of different chemical species across the gas phase, condensed phase, and the interface between them. We demonstrate that SOA nanoparticle growth can be accurately predicted when the relevant thermodynamic and kinetic aspects of aerosol properties, processes, and temperature dependencies are taken into account in an integrative approach of data analysis and numerical modeling.

2 Results and Discussion

Figure 1 illustrates how the elucidation of condensed-phase diffusivity and concentration profiles inside SOA particles resolves previously unexplained discrepancies between field measurements and model predictions of condensable organic vapor concentrations and nanoparticle growth rates. As shown in Fig. 1a and reported by Stolzenburg et al. (2025), nanoparticle growth rates observed in the boreal forest summer (blue markers) were substantially lower than those predicted with a two-film model (Zaveri et al., 2014) assuming quasi-liquid particles with high diffusivity (>10^{-15} cm^2 s^{-1}, solid brown line and shading). In their modeling approach, Stolzenburg et al. (2025) considered uncertainties and variations related to condensable vapor concentration measurements, activity coefficients, decomposition reactions, and reduced diffusivity (10^{-18} cm^2 s^{-1}, dashed brown line), but they did not reach agreement with the measurement results and highlighted incomplete mass closure.

In contrast, our kinetic multilayer model KM3C is able to reproduce the observed growth rates assuming a diffusivity characteristic for highly viscous, nearly glassy semi-solid substances (10^{-20} cm^2 s^{-1}) and otherwise identical model parameters such as the time-dependent concentrations of condensable organic vapors, their enthalpies of vaporization, and the treatment of the Kelvin effect (Supplementary Information, Sects. S1, S2). Using the same diffusivity in the two-film model published by

Stolzenburg et al. (2025), we obtain closure for larger particles sizes, but not below 3 nm (brown dotted line), which indicates that details of interfacial mass transport, molecular diffusion, and differential concentration gradients as resolved in KM3C are relevant for the kinetics of atmospheric nanoparticle growth.

Figure 1c illustrates how low diffusivity leads to the development of differential concentration gradients inside the nanoparticle as described in KM3C, where the outer layers contain higher fractions of relatively more volatile compounds (low-volatile organic compounds, LVOC) compared to the inner layers, which in turn show higher fractions of relatively less volatile compounds (ultra low-volatile organic compounds, ULVOC). This is consistent with the role of ULVOC in new particle formation and nucleation, respectively (Dada et al., 2023; Donahue et al., 2026). The low diffusivity leads to an enrichment of relatively more volatile compounds at the surface, decelerates their uptake into the particle bulk (surface-to-bulk transport), and delays the equilibration of gas-particle partitioning. These effects keep the particle growth rate lower than expected under the assumption of a well-mixed and thus rapidly equilibrating particle phase (Figs. S1, S2).

As illustrated in Fig. 1b, nanoparticle growth observed in the boreal forest spring was well captured by both the two-film model of Stolzenburg et al. (2025) as well as our multilayer model with higher diffusivity (10^{-15} cm^2 s^{-1}, solid blue line and shading). Under these conditions, the multilayer model shows a well-mixed particle bulk without differential concentration gradients (Fig. 1d), indicating that the growth rates observed and simulated under these conditions are not limited by molecular diffusivity. We find that the sensitivity to particle phase state and diffusivity is less pronounced in the springtime scenario (Fig. S3), and KM3C captures the spring data within experimental errors also at a diffusivity of 10^{-18} cm^2 s^{-1} (dashed blue line).

The diffusion properties of complex SOA mixtures have not yet been constrained with high precision, but the occurrence of different phase states and diffusivities of SOA nanoparticles in the investigated growth events is consistent with earlier studies (Virtanen et al., 2010; Saukko et al., 2012; Renbaum-Wolff et al., 2013; Bateman et al., 2016; Shiraiwa et al., 2017; Slade et al., 2019; Kiland et al., 2019; Artaxo et al., 2022; Zhang et al., 2024; Antossian et al., 2026; Golay et al., 2026). To obtain quantitative estimates, we performed model calculations with semi-empirical parameterizations that relate glass transition temperatures, viscosities and self-diffusion coefficients to the volatilities of organic compounds, including particle-size and plasticizer effects (Mikhailov et al., 2013; Cheng et al., 2015; Dette and Koop, 2015; Li et al., 2020; Mahant et al., 2024; Kang et al., 2026). As detailed in the online supplement (Sects. S8, S9), these model calculations support that nanoparticle formation and growth by condensation of low-volatile organic vapors yield particles with very high viscosity and low diffusivity in the range of 10^{-20} to 10^{-18} cm^2 s^{-1}. Due to higher fractions of ULVOC, the diffusivity of newly formed particles in boreal forest air can indeed be lower in summer than in spring (Fig. S5). Despite remaining uncertainties in predicting these properties, our model results demonstrate that kinetic limitations related to particle-phase diffusivity of condensable organic vapors offer a plausible, coherent, and quantitative explanation for previously unexplained observations.

Figure 2 shows nanoparticle growth rates measured under very well defined conditions in the CERN CLOUD chamber (Stolzenburg et al., 2018). For particles in the diameter range of 1.5 to 3 nm (Fig. 2a), the growth rates observed at 5°C are near the kinetic limit derived by Stolzenburg et al. (2025) from the concentration of oxidized organic molecules (OOMs) measured by nitrate chemical ionization mass spectrometry (NO3-CIMS). The rates observed at -25°C and 25°C, however, are well above and below the kinetic limit (OOMs) line, respectively, and were not captured by this modeling approach (Stolzenburg et al.,

2025). In the particle size range of 3 to 7 nm (Fig. 2b), the observed growth rates are close to the reported kinetic limit at 5°C and 25°C, but again much higher at -25°C.

When considering only the OOMs measured by NO3-CIMS (Fig. S7), our kinetic multilayer model was not able to reproduce the observed growth rates. Thus, we included organic vapors measured by proton-transfer reaction time-of-flight mass spectrometry (PTR3; Stolzenburg et al., 2018) and integrated the Clausius-Clapeyron equation in KM3C to describe the temperature-dependent volatility distribution of organic vapors (Supplementary Information, Sect. S1). This approach captures both the concentration dependence and the temperature dependence of the measured nanoparticle growth rates as illustrated in Figs. 2a,b. In accordance with the VBS modeling approach of Stolzenburg et al. (2022), our kinetic model calculations confirm that comprehensive measurement techniques and data are needed to cover the full range and variability of condensable organic vapors. This includes semi-volatile organic compounds (SVOC) that can substantially contribute to nanoparticle growth at -25°C even if their contribution is negligible at +25°C (Fig. S8). As shown by Riva et al. (2019); Mohr et al. (2019); Dada et al. (2023), full coverage of condensable organic vapors by mass spectrometry requires suitable instrumentation and ionization techniques as the sensitivity towards compounds with different degrees of oxygenation can vary strongly. The molecular composition of SOA particles formed by dark ozonolysis of α-pinene (CERN CLOUD) is likely not the same as for particles formed in summertime boreal forest air (Hyytiälä), which may be influenced by other volatile precursors (monoterpenes, sesquiterpenes; Hellén et al., 2018) and photo-oxidants including OH radicals (Baboomian et al., 2022). These differences in aerosol composition and chemical aging can plausibly lead to differences in particle-phase diffusivity (Sect. S5).

Figure 3 shows a wide range of atmospheric nanoparticle growth rates plotted against organic vapor concentrations as observed in the Asian megacity of Beijing (China, Qiao et al., 2021), at the Europe rural background site San Pietro di Capofiume (Italy, Cai et al., 2024), and at the boreal forest site Hyytiälä (Finland, Gonzalez Carracedo et al., 2022) alongside the CERN CLOUD chamber data as presented by Stolzenburg et al. (2025). Similar to the chamber experiments (circular markers), the field measurement data (diamond markers) exhibit a pronounced increase of OOMs concentrations with increasing temperature (color coding), which can be attributed to general trends of temperature-related enhancements in emissions of volatile organic compounds (VOC) as SOA precursors and photochemical reactivity leading to higher OOMs production rates in the atmosphere (Seinfeld and Pandis, 2016; Paasonen et al., 2018; Bianchi et al., 2019). While the OOMs concentrations vary by three orders of magnitude, the nanoparticle growth rates observed in the atmosphere remain rather uniformly confined to a narrow range around 1 to 10 nm h^{-1}.

The field measurement data points and their weak dependence on ambient temperature and measured OOMs concentration do not follow the kinetic-limit line (black dashed) to which they had been related in the recent study of Stolzenburg et al. (2025) highlighting incomplete mass closure of atmospheric nanoparticle growth. In contrast, the solid black fit line to our model results illustrates the weak apparent dependence on OOMs concentration which we obtain using KM3C to predict SOA nanoparticle growth rates as a function of temperature and organic vapor concentration assuming the same volatility distributions as observed in the CERN CLOUD experiments (square markers). The grey shaded areas in Fig. 3 illustrate that most of the growth rates observed in the field measurements and laboratory experiments reported by Stolzenburg et al. (2025) fall within a factor of three relative to this line.

The tilt and flattening of the high OOMs concentration dependence by kinetic-limit lines introduced in earlier studies (Stolzenburg et al., 2018, 2025) towards the weak OOMs concentration dependence indicated by KM3C can be attributed to the following key factors: (I) at low temperature and concentration levels, organic vapors that would have relatively high volatility at room temperature can also contribute to nanoparticle growth (upward shift indicated by the arrow on the left side of Figs. 3a,b); and (II) at high temperature and concentration levels, enhanced volatility, low diffusivity, slow surface-to-bulk transport, and differential concentration gradients decelerate the uptake of organic vapors and delay the equilibration of gas-particle partitioning (downward shift indicated by the arrow on the right side of Figs. 3a,b).

Overall, the variability and temperature dependencies of condensable organic vapor (OOMs) production by VOC oxidation, volatility, and diffusivity are partly offsetting and balancing each other. This balancing leads to an effective buffering of the vapor concentration dependence of atmospheric nanoparticle growth rates around 1 to 10 nm h^{-1} as observed and reported in earlier studies (Kulmala et al., 2004; Kulmala and Kerminen, 2008; Stolzenburg et al., 2023, 2025).

3 Conclusions and Outlook

This study provides an answer to the long-standing and enigmatic scientific question why atmospheric nanoparticle growth rates are fairly uniform under widely different ambient conditions and exhibit a low dependence on organic vapor concentration (OOMs). We have developed and applied a new kinetic multilayer model of multiphase chemistry (KM3C) to explain and reconcile discrepancies between field observations, laboratory experiments, theoretical considerations, and earlier model predictions by resolving the interplay and counteracting effects of temperature-dependent multiphase chemical reactivity, volatility, and diffusivity.

As illustrated in Fig. 4, we identified key factors that lead to an effective buffering and convergence of atmospheric nanoparticle growth rates around 1-10 nm h^{-1} in spite of highly variable ambient conditions, including temperature and organic vapor concentrations. The emission and oxidation of organic compounds that serve as SOA precursors, and the production and concentration of potentially condensable organic vapors in the atmosphere generally tend to increase with increasing temperature. At the same time, however, increasing temperature enhances the volatility and equilibrium vapor pressure of organic compounds, thus reducing the proportions of organic compounds that are actually available to condense under equilibrium conditions in accordance with the Clausius-Clapeyron equation (left side of Fig. 4). On the other hand, increasing proportions of molecules with lower intrinsic volatility can increase the viscosity and reduce the diffusivity of organic aerosols. Low diffusivity in highly viscous, semi-solid or solid particles can decelerate and kinetically limit the uptake and surface-to-bulk transport of organic vapor molecules, generate differential concentration gradients of compounds with different volatilities in the particle, and delay the equilibration of gas-particle partitioning (right side of Fig. 4).

The combination and interplay of these effects can buffer the kinetics of gas-particle partitioning and explain the observation of similar nanoparticle growth rates at vastly differing organic vapor concentrations as observed in well-defined laboratory experiments and ambient air around the world. To reproduce the measurement results, we did not have to invoke chemical reactions in the condensed phase or at the surface of the particles as suggested in related earlier studies (Heitto et al.,

2022; Stolzenburg et al., 2025). Nevertheless, such multiphase chemical reactions - in particular the formation of dimers and oligomers - may also influence the volatility distribution and particle diffusivity, and can be flexibly included in KM3C (Mehra et al., 2020; Berkemeier et al., 2020; Maben and Ziemann, 2023; Kenseth et al., 2023; Schervish et al., 2026; Kang et al., 2026). This also applies for the effects of coagulation and air mass history (Sect. S1; Hussein et al. 2009; Cai et al. 2021; Hakala et al. 2022; Nguyen et al. 2026; Cai et al. 2026).

To further constrain key parameters and enhance the mechanistic understanding and predictability of nanoparticle growth under varying atmospheric conditions, we suggest performing further laboratory experiments and field observations in which nanoparticle composition and phase state are determined alongside condensable vapor concentrations. Future work should quantify the distribution and gradients of organic compounds between and within aerosol particles across the relevant size range. For example, it may be possible to detect or infer radial concentration gradients in highly viscous particles (Huisman et al., 2025; Kang et al., 2026; Schervish et al., 2026) or detect deviations from the composition expected for the uninhibited growth of well-mixed, quasi-liquid particles (Lopez et al., 2025; Bhattacharyya et al., 2025). Kinetic process models, machine learning tools, and targeted uncertainty analysis can help identify the experimental conditions that promise the largest gain of mechanistic understanding (Krüger et al., 2024).

Code and data availability. The measurement data were adopted from Stolzenburg et al. (2018) and Stolzenburg et al. (2025). The KM3C model code is in preparation for public release as open source code.

Author contributions. TB and UP conceived the study. TB designed and supervised research. ZZ, HGK and TB built the kinetic model. ZZ performed kinetic model simulations and processed results. All authors analyzed and discussed the results, and co-wrote the paper led by TB and UP.

Competing interests. At least one of the (co-)authors is a member of the editorial board of ACP.

Acknowledgements. This work was funded by the Max Planck Society (MPG). HGK is supported by the Max Planck Graduate Center with the Johannes Gutenberg University Mainz (MPGC). The authors thank the Max Planck Computing and Data Facility (MPCDF) for computing time on the supercomputer RAVEN. We thank A. Mishra, M. Radecka, and colleagues across the scientific community for helpful discussions.

References

Antossian, C., Müller, M., and Krieger, U. K.: Photochemical and ozone-induced aging significantly alter the viscosity of aqueous *trans*-aconitic acid aerosol particles, Atmos. Chem. Phys., 26, 2443–2463, https://doi.org/10.5194/acp-26-2443-2026, 2026.

Arangio, A. M., Slade, J. H., Berkemeier, T., Pöschl, U., Knopf, D. A., and Shiraiwa, M.: Multiphase Chemical Kinetics of OH Radical Uptake by Molecular Organic Markers of Biomass Burning Aerosols: Humidity and Temperature Dependence, Surface Reaction, and Bulk Diffusion, J. Phys. Chem. A, 119, 4533–4544, https://doi.org/10.1021/jp510489z, 2015.

Artaxo, P., Hansson, H.-C., Andreae, M. O., Bäck, J., Alves, E. G., Barbosa, H. M. J., Bender, F., Bourtsoukidis, E., Carbone, S., Chi, J., Decesari, S., Després, V. R., Ditas, F., Ezhova, E., Fuzzi, S., Hasselquist, N. J., Heintzenberg, J., Holanda, B. A., Guenther, A., Hakola, H., Heikkinen, L., Kerminen, V.-M., Kontkanen, J., Krejci, R., Kulmala, M., Lavric, J. V., de Leeuw, G., Lehtipalo, K., Machado, L. A. T., McFiggans, G., Franco, M. A. M., Meller, B. B., Morais, F. G., Mohr, C., Morgan, W., Nilsson, M. B., Peichl, M., Petäjä, T., Praß, M., Pöhlker, C., Pöhlker, M. L., Pöschl, U., Von Randow, C., Riipinen, I., Rinne, J., Rizzo, L. V., Rosenfeld, D., Silva Dias, M. A. F., Sogacheva, L., Stier, P., Swietlicki, E., Sörgel, M., Tunved, P., Virkkula, A., Wang, J., Weber, B., Yáñez-Serrano, A. M., Zieger, P., Mikhailov, E., Smith, J. N., and Kesselmeier, J.: Tropical and Boreal Forest – Atmosphere Interactions: A Review, Tellus B: Chem. Phys. Meteorol., https://doi.org/10.16993/tellusb.34, 2022.

Baboomian, V. J., Crescenzo, G. V., Huang, Y., Mahrt, F., Shiraiwa, M., Bertram, A. K., and Nizkorodov, S. A.: Sunlight can convert atmospheric aerosols into a glassy solid state and modify their environmental impacts, P. Natl. Acad. Sci. USA, 119, e2208121 119, https://doi.org/10.1073/pnas.2208121119, 2022.

Bateman, A. P., Gong, Z., Liu, P., Sato, B., Cirino, G., Zhang, Y., Artaxo, P., Bertram, A. K., Manzi, A. O., Rizzo, L. V., Souza, R. A. F., Zaveri, R. A., and Martin, S. T.: Sub-micrometre particulate matter is primarily in liquid form over Amazon rainforest, Nat. Geosci., 9, 34–37, https://doi.org/10.1038/ngeo2599, 2016.

Berkemeier, T., Huisman, A. J., Ammann, M., Shiraiwa, M., Koop, T., and Pöschl, U.: Kinetic regimes and limiting cases of gas uptake and heterogeneous reactions in atmospheric aerosols and clouds: a general classification scheme, Atmos. Chem. Phys., 13, 6663–6686, https://doi.org/10.5194/acp-13-6663-2013, 2013.

Berkemeier, T., Shiraiwa, M., Pöschl, U., and Koop, T.: Competition between water uptake and ice nucleation by glassy organic aerosol particles, Atmos. Chem. Phys., 14, 12 513–12 531, https://doi.org/10.5194/acp-14-12513-2014, 2014.

Berkemeier, T., Steimer, S. S., Krieger, U. K., Peter, T., Pöschl, U., Ammann, M., and Shiraiwa, M.: Ozone uptake on glassy, semi-solid and liquid organic matter and the role of reactive oxygen intermediates in atmospheric aerosol chemistry, Phys. Chem. Chem. Phys., 18, 12 662–12 674, https://doi.org/10.1039/C6CP00634E, 2016.

Berkemeier, T., Takeuchi, M., Eris, G., and Ng, N. L.: Kinetic modeling of formation and evaporation of secondary organic aerosol from NO_3 oxidation of pure and mixed monoterpenes, Atmos. Chem. Phys., 20, 15 513–15 535, https://doi.org/10.5194/acp-20-15513-2020, 2020.

Bhattacharyya, N., Lopez, B., DeVivo, J., Russell, D. M., Shen, J., Sommer, E., Almeida, J., Amorim, A., Beckmann, H. M., Busato, M., Canagaratna, M. R., Caudillo, L., Chassaing, A., Christoudias, T., Dada, L., El-Haddad, I., Flagan, R. C., Harder, H., Judmaier, B., Kaniyodical Sebastian, M., Kirkby, J., Klebach, H., Kulmala, M., Kunkler, F., Lehtipalo, K., Liu, L., Mentler, B., Möhler, O., Morawiec, A., Petäjä, T., Rato, P., Rörup, B., Ruhl, S., Scholz, W., Simon, M., Tóme, A., Tong, Y., Top, J., Umo, N. S., Volkamer, R., Weissbacher, J., Worsnop, D. R., Xenofontos, C., Yang, B., Yu, W., Zauner-Wieczorek, M., Zgheib, I., Zhang, J., Zheng, Z., He, X.-C., Stolzenburg, D., Schobesberger, S., Curtius, J., and Donahue, N. M.: Isoprene Aerosol Growth in the Upper Troposphere: Application of the Diagonal Volatility Basis Set to CLOUD Chamber Measurements, ACS ES&T Air, 2, 2092–2104, https://doi.org/10.1021/acsestair.5c00106, 2025.

Bianchi, F., Tröstl, J., Junninen, H., Frege, C., Henne, S., Hoyle, C. R., Molteni, U., Herrmann, E., Adamov, A., Bukowiecki, N., Chen, X., Duplissy, J., Gysel, M., Hutterli, M., Kangasluoma, J., Kontkanen, J., Kürten, A., Manninen, H. E., Münch, S., Peräkylä, O., Petäjä, T., Rondo, L., Williamson, C., Weingartner, E., Curtius, J., Worsnop, D. R., Kulmala, M., Dommen, J., and Baltensperger, U.: New particle formation in the free troposphere: A question of chemistry and timing, Science, 352, 1109–1112, https://doi.org/10.1126/science.aad5456, 2016.

Bianchi, F., Kurtén, T., Riva, M., Mohr, C., Rissanen, M. P., Roldin, P., Berndt, T., Crounse, J. D., Wennberg, P. O., Mentel, T. F., Wildt, J., Junninen, H., Jokinen, T., Kulmala, M., Worsnop, D. R., Thornton, J. A., Donahue, N., Kjaergaard, H. G., and Ehn, M.: Highly Oxygenated Organic Molecules (HOM) from Gas-Phase Autoxidation Involving Peroxy Radicals: A Key Contributor to Atmospheric Aerosol, Chem. Rev., 119, 3472–3509, https://doi.org/10.1021/acs.chemrev.8b00395, 2019.

Cai, J., Sulo, J., Gu, Y., Holm, S., Cai, R., Thomas, S., Neuberger, A., Mattsson, F., Paglione, M., Decesari, S., Rinaldi, M., Yin, R., Aliaga, D., Huang, W., Li, Y., Gramlich, Y., Ciarelli, G., Quéléver, L., Sarnela, N., Lehtipalo, K., Zannoni, N., Wu, C., Nie, W., Kangasluoma, J., Mohr, C., Kulmala, M., Zha, Q., Stolzenburg, D., and Bianchi, F.: Elucidating the mechanisms of atmospheric new particle formation in the highly polluted Po Valley, Italy, Atmos. Chem. Phys., 24, 2423–2441, https://doi.org/10.5194/acp-24-2423-2024, 2024.

Cai, R., Li, C., He, X.-C., Deng, C., Lu, Y., Yin, R., Yan, C., Wang, L., Jiang, J., Kulmala, M., and Kangasluoma, J.: Impacts of coagulation on the appearance time method for new particle growth rate evaluation and their corrections, Atmos. Chem. Phys., 21, 2287–2304, https://doi.org/10.5194/acp-21-2287-2021, 2021.

Cai, R., Li, X., Li, Y., Blichner, S., Stolzenburg, D., Zha, Q., Cai, J., Nie, W., Yan, C., Huang, D. D., Wang, Z., Wu, J., Yin, R., Sarnela, N., Huang, W., Tuovinen, S., Holm, S., Ahonen, L., Yao, L., Ding, A., Bianchi, F., Liu, Y., Winkler, P. M., Petäjä, T., Chen, J., Kerminen, V.-M., Wang, L., Worsnop, D., Jiang, J., Kulmala, M., and Kangasluoma, J.: The key role of nanoparticle concentration gradient in aerosol initial growth, Nat. Commun., https://doi.org/10.1038/s41467-026-70082-2, 2026.

Cheng, Y., Su, H., Koop, T., Mikhailov, E., and Pöschl, U.: Size dependence of phase transitions in aerosol nanoparticles, Nat. Commun., 6, 5923, https://doi.org/10.1038/ncomms6923, 2015.

Dada, L., Stolzenburg, D., Simon, M., Fischer, L., Heinritzi, M., Wang, M., Xiao, M., Vogel, A. L., Ahonen, L., Amorim, A., Baalbaki, R., Baccarini, A., Baltensperger, U., Bianchi, F., Daellenbach, K. R., DeVivo, J., Dias, A., Dommen, J., Duplissy, J., Finkenzeller, H., Hansel, A., He, X.-C., Hofbauer, V., Hoyle, C. R., Kangasluoma, J., Kim, C., Kürten, A., Kvashnin, A., Mauldin, R., Makhmutov, V., Marten, R., Mentler, B., Nie, W., Petäjä, T., Quéléver, L. L. J., Saathoff, H., Tauber, C., Tome, A., Molteni, U., Volkamer, R., Wagner, R., Wagner, A. C., Wimmer, D., Winkler, P. M., Yan, C., Zha, Q., Rissanen, M., Gordon, H., Curtius, J., Worsnop, D. R., Lehtipalo, K., Donahue, N. M., Kirkby, J., El Haddad, I., and Kulmala, M.: Role of sesquiterpenes in biogenic new particle formation, Sci. Adv., 9, https://doi.org/10.1126/sciadv.adi5297, 2023.

Dette, H. P. and Koop, T.: Glass Formation Processes in Mixed Inorganic/Organic Aerosol Particles, J. Phys. Chem. A, 119, 4552–4561, https://doi.org/10.1021/jp5106967, 2015.

Donahue, N. M., Robinson, A. L., Stanier, C. O., and Pandis, S. N.: Coupled Partitioning, Dilution, and Chemical Aging of Semivolatile Organics, Environ. Sci. Technol., 40, 2635–2643, https://doi.org/10.1021/es052297c, 2006.

Donahue, N. M., Epstein, S. A., Pandis, S. N., and Robinson, A. L.: A two-dimensional volatility basis set: 1. organic-aerosol mixing thermodynamics, Atmos. Chem. Phys., 11, 3303–3318, https://doi.org/10.5194/acp-11-3303-2011, 2011.

Donahue, N. M., Dada, L., Stolzenburg, D., Sommer, E., Simon, M., Schervish, M., DeVivo, J., Stinchfield, A., Burton, N., Bhattacharyya, N., Lopez, B., Wang, M., Scholz, W., Almeida, J., Zhao, B., Heinritzi, M., Gordon, H., Hansel, A., Curtius, J., Lehtipalo, K., El Haddad,

I., Kirkby, J., Flagan, R., Kulmala, M., and Worsnop, D.: On describing particle nucleation within the Volatility Basis Set, Atmos. Chem. Phys., 26, 8311–8339, https://doi.org/10.5194/acp-26-8311-2026, 2026.

Golay, Z. M., Vandergrift, G. W., Kamal, S., China, S., Nizkorodov, S. A., and Bertram, A. K.: Sunlight can turn smoldering pine wood smoke into a glass, npj Clean Air, 2, 29, https://doi.org/10.1038/s44407-026-00070-9, 2026.

Gonzalez Carracedo, L., Lehtipalo, K., Ahonen, L. R., Sarnela, N., Holm, S., Kangasluoma, J., Kulmala, M., Winkler, P. M., and Stolzenburg, D.: On the relation between apparent ion and total particle growth rates in the boreal forest and related chamber experiments, Atmos. Chem. Phys., 22, 13 153–13 166, https://doi.org/10.5194/acp-22-13153-2022, 2022.

Gordon, H., Kirkby, J., Baltensperger, U., Bianchi, F., Breitenlechner, M., Curtius, J., Dias, A., Dommen, J., Donahue, N. M., Dunne, E. M., Duplissy, J., Ehrhart, S., Flagan, R. C., Frege, C., Fuchs, C., Hansel, A., Hoyle, C. R., Kulmala, M., Kürten, A., Lehtipalo, K., Makhmutov, V., Molteni, U., Rissanen, M. P., Stozkhov, Y., Tröstl, J., Tsagkogeorgas, G., Wagner, R., Williamson, C., Wimmer, D., Winkler, P. M., Yan, C., and Carslaw, K. S.: Causes and importance of new particle formation in the present-day and preindustrial atmospheres, J. Geophys. Res.: Atmos., 122, 8739–8760, https://doi.org/10.1002/2017jd026844, 2017.

Hakala, S., Vakkari, V., Bianchi, F., Dada, L., Deng, C., Dällenbach, K. R., Fu, Y., Jiang, J., Kangasluoma, J., Kujansuu, J., Liu, Y., Petäjä, T., Wang, L., Yan, C., Kulmala, M., and Paasonen, P.: Observed coupling between air mass history, secondary growth of nucleation mode particles and aerosol pollution levels in Beijing, Environ. Sci.: Atmos., 2, 146–164, https://doi.org/10.1039/d1ea00089f, 2022.

Hallquist, M., Wenger, J. C., Baltensperger, U., Rudich, Y., Simpson, D., Claeys, M., Dommen, J., Donahue, N. M., George, C., Goldstein, A. H., Hamilton, J. F., Herrmann, H., Hoffmann, T., Iinuma, Y., Jang, M., Jenkin, M. E., Jimenez, J. L., Kiendler-Scharr, A., Maenhaut, W., McFiggans, G., Mentel, T. F., Monod, A., Prévôt, A. S. H., Seinfeld, J. H., Surratt, J. D., Szmigielski, R., and Wildt, J.: The formation, properties and impact of secondary organic aerosol: current and emerging issues, Atmos. Chem. Phys., 9, 5155–5236, https://doi.org/10.5194/acp-9-5155-2009, 2009.

Heitto, A., Lehtinen, K., Petäjä, T., Lopez-Hilfiker, F., Thornton, J. A., Kulmala, M., and Yli-Juuti, T.: Effects of oligomerization and decomposition on the nanoparticle growth: a model study, Atmos. Chem. Phys., 22, 155–171, https://doi.org/10.5194/acp-22-155-2022, 2022.

Hellén, H., Praplan, A. P., Tykkä, T., Ylivinkka, I., Vakkari, V., Bäck, J., Petäjä, T., Kulmala, M., and Hakola, H.: Long-term measurements of volatile organic compounds highlight the importance of sesquiterpenes for the atmospheric chemistry of a boreal forest, Atmos. Chem. Phys., 18, 13 839–13 863, https://doi.org/10.5194/acp-18-13839-2018, 2018.

Huisman, M., Poon, W. C. K., Warren, P. B., Titmuss, S., and Marenduzzo, D.: Diffusive evaporation dynamics in polymer solutions is ubiquitous, Soft Matter, 21, 1508–1515, https://doi.org/10.1039/D4SM01215A, 2025.

Hussein, T., Junninen, H., Tunved, P., Kristensson, A., Dal Maso, M., Riipinen, I., Aalto, P. P., Hansson, H.-C., Swietlicki, E., and Kulmala, M.: Time span and spatial scale of regional new particle formation events over Finland and Southern Sweden, Atmos. Chem. Phys., 9, 4699–4716, https://doi.org/10.5194/acp-9-4699-2009, 2009.

IPCC: Climate Change 2023: Synthesis Report. Contribution of Working Groups I, II and III to the Sixth Assessment Report of the Intergovernmental Panel on Climate Change, https://doi.org/10.59327/IPCC/AR6-9789291691647, 2023.

Jimenez, J. L., Canagaratna, M. R., Donahue, N. M., Prevot, A. S. H., Zhang, Q., Kroll, J. H., DeCarlo, P. F., Allan, J. D., Coe, H., Ng, N. L., Aiken, A. C., Docherty, K. S., Ulbrich, I. M., Grieshop, A. P., Robinson, A. L., Duplissy, J., Smith, J. D., Wilson, K. R., Lanz, V. A., Hueglin, C., Sun, Y. L., Tian, J., Laaksonen, A., Raatikainen, T., Rautiainen, J., Vaattovaara, P., Ehn, M., Kulmala, M., Tomlinson, J. M., Collins, D. R., Cubison, M. J., Dunlea, J., Huffman, J. A., Onasch, T. B., Alfarra, M. R., Williams, P. I., Bower, K., Kondo, Y., Schneider, J., Drewnick, F., Borrmann, S., Weimer, S., Demerjian, K., Salcedo, D., Cottrell, L., Griffin, R., Takami, A., Miyoshi, T., Hatakeyama, S.,

Shimono, A., Sun, J. Y., Zhang, Y. M., Dzepina, K., Kimmel, J. R., Sueper, D., Jayne, J. T., Herndon, S. C., Trimborn, A. M., Williams, L. R., Wood, E. C., Middlebrook, A. M., Kolb, C. E., Baltensperger, U., and Worsnop, D. R.: Evolution of Organic Aerosols in the Atmosphere, Science, 326, 1525–1529, https://doi.org/10.1126/science.1180353, 2009.

Kang, H. G., Takeuchi, M., Ng, N. L., Pöschl, U., and Berkemeier, T.: Multiphase Chemistry and Phase State Explain Nonlinear Effects in the Formation and Evaporation of SOA from Mixed Monoterpene Precursors, ACS ES&T Air, https://doi.org/10.1021/acsestair.5c00438, 2026.

Kenseth, C. M., Hafeman, N. J., Rezgui, S. P., Chen, J., Huang, Y., Dalleska, N. F., Kjaergaard, H. G., Stoltz, B. M., Seinfeld, J. H., and Wennberg, P. O.: Particle-phase accretion forms dimer esters in pinene secondary organic aerosol, Science, 382, 787–792, https://doi.org/10.1126/science.adi0857, 2023.

Kiland, K. J., Maclean, A. M., Kamal, S., and Bertram, A. K.: Diffusion of Organic Molecules as a Function of Temperature in a Sucrose Matrix (a Proxy for Secondary Organic Aerosol), J. Phys. Chem. Lett., 10, 5902–5908, https://doi.org/10.1021/acs.jpclett.9b02182, 2019.

Koop, T., Bookhold, J., Shiraiwa, M., and Pöschl, U.: Glass transition and phase state of organic compounds: dependency on molecular properties and implications for secondary organic aerosols in the atmosphere, Phys. Chem. Chem. Phys., 13, 19 238, https://doi.org/10.1039/c1cp22617g, 2011.

Krüger, M., Mishra, A., Spichtinger, P., Pöschl, U., and Berkemeier, T.: A numerical compass for experiment design in chemical kinetics and molecular property estimation, J. Cheminf., 16, 34, https://doi.org/10.1186/s13321-024-00825-0, 2024.

Kulmala, M. and Kerminen, V.-M.: On the formation and growth of atmospheric nanoparticles, Atmos. Res., 90, 132–150, https://doi.org/https://doi.org/10.1016/j.atmosres.2008.01.005, 2008.

Kulmala, M., Vehkamäki, H., Petäjä, T., Dal Maso, M., Lauri, A., Kerminen, V.-M., Birmili, W., and McMurry, P.: Formation and growth rates of ultrafine atmospheric particles: a review of observations, J. Aerosol Sci., 35, 143–176, https://doi.org/10.1016/j.jaerosci.2003.10.003, 2004.

Kulmala, M., Petäjä, T., Ehn, M., Thornton, J., Sipilä, M., Worsnop, D., and Kerminen, V.-M.: Chemistry of Atmospheric Nucleation: On the Recent Advances on Precursor Characterization and Atmospheric Cluster Composition in Connection with Atmospheric New Particle Formation, Annu. Rev. Phys. Chem., 65, 21–37, https://doi.org/10.1146/annurev-physchem-040412-110014, 2014.

Kulmala, M., Cai, R., Stolzenburg, D., Zhou, Y., Dada, L., Guo, Y., Yan, C., Petäjä, T., Jiang, J., and Kerminen, V.-M.: The contribution of new particle formation and subsequent growth to haze formation, Environ. Sci.: Atmos., 2, 352–361, https://doi.org/10.1039/D1EA00096A, 2022.

Li, Y., Day, D. A., Stark, H., Jimenez, J. L., and Shiraiwa, M.: Predictions of the glass transition temperature and viscosity of organic aerosols from volatility distributions, Atmos. Chem. Phys., 20, 8103–8122, https://doi.org/10.5194/acp-20-8103-2020, 2020.

Li, Y., Heald, C. L., Miao, R., Campuzano-Jost, P., and Jimenez, J. L.: Global Impacts of Simulating Organic Aerosol Phase State, Environ. Sci. Technol., https://doi.org/10.1021/acs.est.5c13238, 2026.

Lopez, B., Bhattacharyya, N., DeVivo, J., Wang, M., Caudillo-Plath, L., Surdu, M., Bianchi, F., Brasseur, Z., Buchholz, A., Chen, D., Duplissy, J., He, X.-C., Hofbauer, V., Mahfouz, N., Makhmutov, V., Marten, R., Mentler, B., Philippov, M., Schervish, M., Wang, D. S., Weber, S. K., Welti, A., El Haddad, I., Lehtipalo, K., Kulmala, M., Worsnop, D., Kirkby, J., Mauldin, R. L., Stolzenburg, D., Schobesberger, S., Flagan, R., and Donahue, N. M.: A diagonal volatility basis set to assess the condensation of organic vapors onto particles, Environ. Sci.: Atmos., 5, 1035–1061, https://doi.org/10.1039/d5ea00062a, 2025.

Maben, H. K. and Ziemann, P. J.: Kinetics of oligomer-forming reactions involving the major functional groups present in atmospheric secondary organic aerosol particles, Environ. Sci.: Processes Impacts, 25, 214–228, https://doi.org/10.1039/D2EM00124A, 2023.

Mahant, S., Snider, J. R., Petters, S. S., and Petters, M. D.: Effect of Aerosol Size on Glass Transition Temperature, J. Phys. Chem. Lett., 15, 7509–7515, https://doi.org/10.1021/acs.jpclett.4c01415, 2024.

Mehra, A., Krechmer, J. E., Lambe, A., Sarkar, C., Williams, L., Khalaj, F., Guenther, A., Jayne, J., Coe, H., Worsnop, D., Faiola, C., and Canagaratna, M.: Oligomer and highly oxygenated organic molecule formation from oxidation of oxygenated monoterpenes emitted by California sage plants, Atmos. Chem. Phys., 20, 10 953–10 965, https://doi.org/10.5194/acp-20-10953-2020, 2020.

Mikhailov, E., Vlasenko, S., Martin, S. T., Koop, T., and Pöschl, U.: Amorphous and crystalline aerosol particles interacting with water vapor: conceptual framework and experimental evidence for restructuring, phase transitions and kinetic limitations, Atmos. Chem. Phys., 9, 9491–9522, https://doi.org/10.5194/acp-9-9491-2009, 2009.

Mikhailov, E., Vlasenko, S., Rose, D., and Pöschl, U.: Mass-based hygroscopicity parameter interaction model and measurement of atmospheric aerosol water uptake, Atmos. Chem. Phys., 13, 717–740, https://doi.org/10.5194/acp-13-717-2013, 2013.

Mohr, C., Thornton, J. A., Heitto, A., Lopez-Hilfiker, F. D., Lutz, A., Riipinen, I., Hong, J., Donahue, N. M., Hallquist, M., Petäjä, T., Kulmala, M., and Yli-Juuti, T.: Molecular identification of organic vapors driving atmospheric nanoparticle growth, Nat. Commun., 10, https://doi.org/10.1038/s41467-019-12473-2, 2019.

Mu, Q., Shiraiwa, M., Octaviani, M., Ma, N., Ding, A., Su, H., Lammel, G., Pöschl, U., and Cheng, Y.: Temperature effect on phase state and reactivity controls atmospheric multiphase chemistry and transport of PAHs, Sci. Adv., 4, eaap7314, https://doi.org/10.1126/sciadv.aap7314, 2018.

Nguyen, K., Schervish, M., Lakey, P. S. J., Smith, J. N., and Shiraiwa, M.: Impact of particle phase state on the competition between condensation and coagulation, Environ. Sci.: Atmos., 6, 152–165, https://doi.org/10.1039/d5ea00069f, 2026.

Paasonen, P., Peltola, M., Kontkanen, J., Junninen, H., Kerminen, V.-M., and Kulmala, M.: Comprehensive analysis of particle growth rates from nucleation mode to cloud condensation nuclei in boreal forest, Atmos. Chem. Phys., 18, 12 085–12 103, https://doi.org/10.5194/acp-18-12085-2018, 2018.

Pfrang, C., Shiraiwa, M., and Pöschl, U.: Chemical ageing and transformation of diffusivity in semi-solid multi-component organic aerosol particles, Atmos. Chem. Phys., 11, 7343–7354, https://doi.org/10.5194/acp-11-7343-2011, 2011.

Qiao, X., Yan, C., Li, X., Guo, Y., Yin, R., Deng, C., Li, C., Nie, W., Wang, M., Cai, R., Huang, D., Wang, Z., Yao, L., Worsnop, D. R., Bianchi, F., Liu, Y., Donahue, N. M., Kulmala, M., and Jiang, J.: Contribution of Atmospheric Oxygenated Organic Compounds to Particle Growth in an Urban Environment, Environ. Sci. Technol., 55, 13 646–13 656, https://doi.org/10.1021/acs.est.1c02095, 2021.

Reid, J. P., Bertram, A. K., Topping, D. O., Laskin, A., Martin, S. T., Petters, M. D., Pope, F. D., and Rovelli, G.: The viscosity of atmospherically relevant organic particles, Nat. Commun., 9, 956, https://doi.org/10.1038/s41467-018-03027-z, 2018.

Renbaum-Wolff, L., Grayson, J. W., Bateman, A. P., Kuwata, M., Sellier, M., Murray, B. J., Shilling, J. E., Martin, S. T., and Bertram, A. K.: Viscosity of α-pinene secondary organic material and implications for particle growth and reactivity, P. Natl. Acad. Sci. USA, 110, 8014–8019, https://doi.org/10.1073/pnas.1219548110, 2013.

Riipinen, I., Pierce, J. R., Yli-Juuti, T., Nieminen, T., Häkkinen, S., Ehn, M., Junninen, H., Lehtipalo, K., Petäjä, T., Slowik, J., Chang, R., Shantz, N. C., Abbatt, J., Leaitch, W. R., Kerminen, V.-M., Worsnop, D. R., Pandis, S. N., Donahue, N. M., and Kulmala, M.: Organic condensation: a vital link connecting aerosol formation to cloud condensation nuclei (CCN) concentrations, Atmos. Chem. Phys., 11, 3865–3878, https://doi.org/10.5194/acp-11-3865-2011, 2011.

Riva, M., Rantala, P., Krechmer, J. E., Peräkylä, O., Zhang, Y., Heikkinen, L., Garmash, O., Yan, C., Kulmala, M., Worsnop, D., and Ehn, M.: Evaluating the performance of five different chemical ionization techniques for detecting gaseous oxygenated organic species, Atmos. Meas. Tech., 12, 2403–2421, https://doi.org/10.5194/amt-12-2403-2019, 2019.

Saukko, E., Lambe, A. T., Massoli, P., Koop, T., Wright, J. P., Croasdale, D. R., Pedernera, D. A., Onasch, T. B., Laaksonen, A., Davidovits, P., Worsnop, D. R., and Virtanen, A.: Humidity-dependent phase state of SOA particles from biogenic and anthropogenic precursors, Atmos. Chem. Phys., 12, 7517–7529, https://doi.org/10.5194/acp-12-7517-2012, 2012.

Schervish, M., Kang, H. G., Wingen, L. M., Nguyen, K., Begay, C., Wilson, J., Shrivastava, M., Chen, Y., Shilling, J. E., Ng, N. L., Pöschl, U., Berkemeier, T., Zelenyuk, A., and Shiraiwa, M.: Surface Crust Formation Controls Evaporation Kinetics of Secondary Organic Aerosols, Environ. Sci. Technol., 60, 7995–8006, https://doi.org/10.1021/acs.est.5c11018, 2026.

Seinfeld, J. H. and Pandis, S. N.: Atmospheric chemistry and physics: from air pollution to climate change, John Wiley & Sons, 2016.

Shiraiwa, M., Ammann, M., Koop, T., and Pöschl, U.: Gas uptake and chemical aging of semisolid organic aerosol particles, P. Natl. Acad. Sci. USA, 108, 11 003–11 008, https://doi.org/10.1073/pnas.1103045108, 2011.

Shiraiwa, M., Berkemeier, T., Schilling-Fahnestock, K. A., Seinfeld, J. H., and Pöschl, U.: Molecular corridors and kinetic regimes in the multiphase chemical evolution of secondary organic aerosol, Atmos. Chem. Phys., 14, 8323–8341, https://doi.org/10.5194/acp-14-8323-2014, 2014.

Shiraiwa, M., Li, Y., Tsimpidi, A. P., Karydis, V. A., Berkemeier, T., Pandis, S. N., Lelieveld, J., Koop, T., and Pöschl, U.: Global distribution of particle phase state in atmospheric secondary organic aerosols, Nat. Commun., 8, 15 002, https://doi.org/10.1038/ncomms15002, 2017.

Shrivastava, M., Cappa, C. D., Fan, J., Goldstein, A. H., Guenther, A. B., Jimenez, J. L., Kuang, C., Laskin, A., Martin, S. T., Ng, N. L., Petaja, T., Pierce, J. R., Rasch, P. J., Roldin, P., Seinfeld, J. H., Shilling, J., Smith, J. N., Thornton, J. A., Volkamer, R., Wang, J., Worsnop, D. R., Zaveri, R. A., Zelenyuk, A., and Zhang, Q.: Recent advances in understanding secondary organic aerosol: Implications for global climate forcing, Rev. Geophys., 55, 509–559, https://doi.org/10.1002/2016RG000540, 2017.

Slade, J. H., Ault, A. P., Bui, A. T., Ditto, J. C., Lei, Z., Bondy, A. L., Olson, N. E., Cook, R. D., Desrochers, S. J., Harvey, R. M., Erickson, M. H., Wallace, H. W., Alvarez, S. L., Flynn, J. H., Boor, B. E., Petrucci, G. A., Gentner, D. R., Griffin, R. J., and Shepson, P. B.: Bouncier Particles at Night: Biogenic Secondary Organic Aerosol Chemistry and Sulfate Drive Diel Variations in the Aerosol Phase in a Mixed Forest, Environ. Sci. Technol., 53, 4977–4987, https://doi.org/10.1021/acs.est.8b07319, pMID: 31002496, 2019.

Stolzenburg, D., Fischer, L., Vogel, A. L., Heinritzi, M., Schervish, M., Simon, M., Wagner, A. C., Dada, L., Ahonen, L. R., Amorim, A., Baccarini, A., Bauer, P. S., Baumgartner, B., Bergen, A., Bianchi, F., Breitenlechner, M., Brilke, S., Buenrostro Mazon, S., Chen, D., Dias, A., Draper, D. C., Duplissy, J., El Haddad, I., Finkenzeller, H., Frege, C., Fuchs, C., Garmash, O., Gordon, H., He, X., Helm, J., Hofbauer, V., Hoyle, C. R., Kim, C., Kirkby, J., Kontkanen, J., Kürten, A., Lampilahti, J., Lawler, M., Lehtipalo, K., Leiminger, M., Mai, H., Mathot, S., Mentler, B., Molteni, U., Nie, W., Nieminen, T., Nowak, J. B., Ojdanic, A., Onnela, A., Passananti, M., Petäjä, T., Quéléver, L. L. J., Rissanen, M. P., Sarnela, N., Schallhart, S., Tauber, C., Tomé, A., Wagner, R., Wang, M., Weitz, L., Wimmer, D., Xiao, M., Yan, C., Ye, P., Zha, Q., Baltensperger, U., Curtius, J., Dommen, J., Flagan, R. C., Kulmala, M., Smith, J. N., Worsnop, D. R., Hansel, A., Donahue, N. M., and Winkler, P. M.: Rapid growth of organic aerosol nanoparticles over a wide tropospheric temperature range, P. Natl. Acad. Sci. USA, 115, 9122–9127, https://doi.org/10.1073/pnas.1807604115, 2018.

Stolzenburg, D., Wang, M., Schervish, M., and Donahue, N. M.: Tutorial: Dynamic organic growth modeling with a volatility basis set, J. Aerosol Sci., 166, 106 063, https://doi.org/10.1016/j.jaerosci.2022.106063, 2022.

Stolzenburg, D., Cai, R., Blichner, S. M., Kontkanen, J., Zhou, P., Makkonen, R., Kerminen, V.-M., Kulmala, M., Riipinen, I., and Kangasluoma, J.: Atmospheric nanoparticle growth, Rev. Mod. Phys., 95, 045 002, https://doi.org/10.1103/RevModPhys.95.045002, 2023.

Stolzenburg, D., Sarnela, N., Bianchi, F., Cai, J., Cai, R., Cheng, Y., Dada, L., Donahue, N. M., Grothe, H., Holm, S., Kerminen, V.-M., Lehtipalo, K., Petäjä, T., Sulo, J., Winkler, P. M., Yan, C., Kangasluoma, J., and Kulmala, M.: Incomplete mass closure in atmospheric nanoparticle growth, npj Clim. Atmos. Sci., 8, https://doi.org/10.1038/s41612-025-00893-5, 2025.

Virtanen, A., Joutsensaari, J., Koop, T., Kannosto, J., Yli-Pirilä, P., Leskinen, J., Mäkelä, J. M., Holopainen, J. K., Pöschl, U., Kulmala, M., Worsnop, D. R., and Laaksonen, A.: An amorphous solid state of biogenic secondary organic aerosol particles, Nature, 467, 824–827, https://doi.org/10.1038/nature09455, 2010.

WHO: Health workforce support and safeguards list 2023, Tech. rep., World Health Organization, Geneva, Switzerland, https://www.who.int/publications/i/item/9789240069787, accessed: 2026 April 1, 2023.

Yli-Juuti, T., Mohr, C., and Riipinen, I.: Open questions on atmospheric nanoparticle growth, Commun. Chem., 3, 106, https://doi.org/10.1038/s42004-020-00339-4, 2020.

Zaveri, R. A., Easter, R. C., Shilling, J. E., and Seinfeld, J. H.: Modeling kinetic partitioning of secondary organic aerosol and size distribution dynamics: representing effects of volatility, phase state, and particle-phase reaction, Atmos. Chem. Phys., 14, 5153–5181, https://doi.org/10.5194/acp-14-5153-2014, 2014.

Zaveri, R. A., Shilling, J. E., Zelenyuk, A., Liu, J., Bell, D. M., D'Ambro, E. L., Gaston, C. J., Thornton, J. A., Laskin, A., Lin, P., Wilson, J., Easter, R. C., Wang, J., Bertram, A. K., Martin, S. T., Seinfeld, J. H., and Worsnop, D. R.: Growth Kinetics and Size Distribution Dynamics of Viscous Secondary Organic Aerosol, Environ. Sci. Technol., 52, 1191–1199, https://doi.org/10.1021/acs.est.7b04623, 2018.

Zaveri, R. A., Shilling, J. E., Zelenyuk, A., Zawadowicz, M. A., Suski, K., China, S., Bell, D. M., Veghte, D., and Laskin, A.: Particle-Phase Diffusion Modulates Partitioning of Semivolatile Organic Compounds to Aged Secondary Organic Aerosol, Environ. Sci. Technol., 54, 2595–2605, https://doi.org/10.1021/acs.est.9b05514, 2020.

Zhang, Z., Li, Y., Ran, H., An, J., Qu, Y., Zhou, W., Xu, W., Hu, W., Xie, H., Wang, Z., Sun, Y., and Shiraiwa, M.: Simulated phase state and viscosity of secondary organic aerosols over China, Atmos. Chem. Phys., 24, 4809–4826, https://doi.org/10.5194/acp-24-4809-2024, 2024.

Zhou, S., Shiraiwa, M., McWhinney, R. D., Pöschl, U., and Abbatt, J. P. D.: Kinetic limitations in gas-particle reactions arising from slow diffusion in secondary organic aerosol, Faraday Discuss., 165, 391–406, https://doi.org/10.1039/C3FD00030C, 2013.

Zobrist, B., Marcolli, C., Pedernera, D. A., and Koop, T.: Do atmospheric aerosols form glasses?, Atmos. Chem. Phys., 8, 5221–5244, https://doi.org/10.5194/acp-8-5221-2008, 2008.

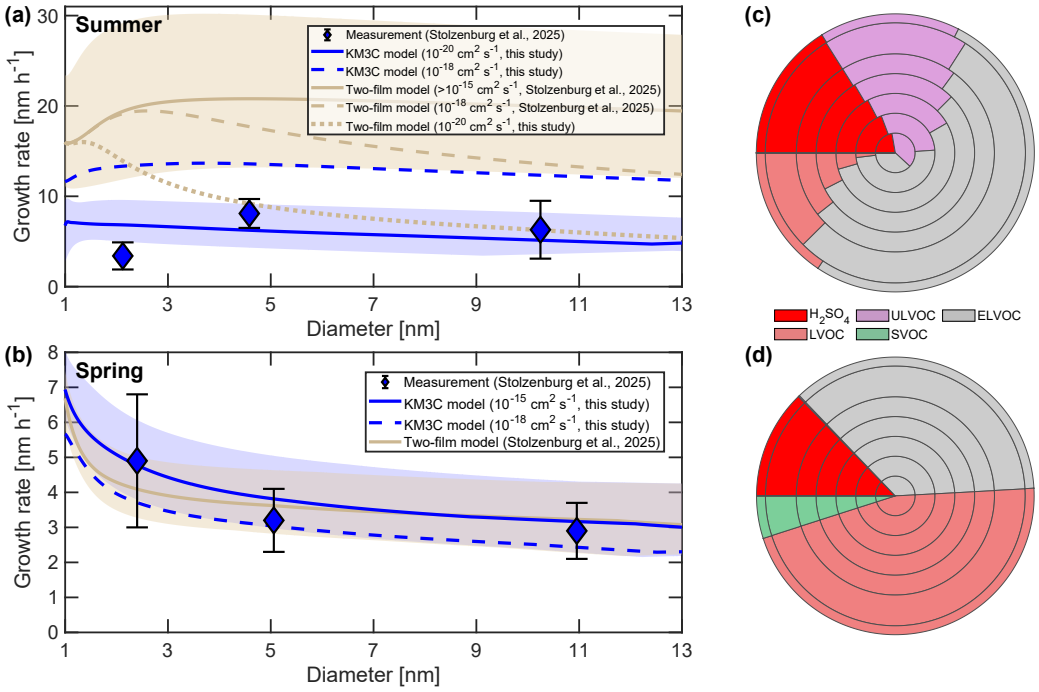

Figure 1. Atmospheric nanoparticle growth observed in field measurements. Blue diamond markers and error bars represent arithmetic mean values and standard deviations of growth rates measured in **(a)** summer and **(b)** spring at a boreal forest site (Hyytiälä, Finland; Gonzalez Carracedo et al. (2022)). Lines and shadings represent model predictions and uncertainty ranges obtained with a traditional two-film model in brown color (Stolzenburg et al., 2025) and with the new multilayer model KM3C in blue color (Sect. S4). KM3C captures the observations assuming low diffusivity (10^{-20} cm^2 s^{-1}) in summer **(a)** and high diffusivity (10^{-15} cm^2 s^{-1}) in spring **(b)**. With the high and intermediate diffusivities assumed by Stolzenburg et al. (2025), the two-film model matches the observations in spring but not in summer (>10^{-15} cm^2 s^{-1}, solid brown line; 10^{-18} cm^2 s^{-1}, dashed brown line). Inserting the same low diffusivity as in KM3C (10^{-20} cm^2 s^{-1}), the two-film model can also match the summertime observations data for particles larger than 4 nm (dotted line). Note that all diffusivities listed for KM3C represent values at 298 K that are adjusted for temperature with $E_{\mathrm{a,dif}} = 40$ kJ mol^{-1} in the model, while diffusivities in the two-film model are kept at their nominal values. Radial concentration profiles of sulfuric acid (H_2SO_4) and organic compounds with different volatilities (ULVOC, ELVOC, LVOC, SVOC) calculated by KM3C show that the growing particles (7 nm) are well-mixed and contain larger proportions of more volatile compounds (LVOC/SVOC) in spring **(d)**. In summer **(c)**, however, the growing particles contain larger proportions of less volatile compounds (ULVOC/ELVOC) and exhibit differential concentration gradients, which reflect kinetic limitations of mass transport.

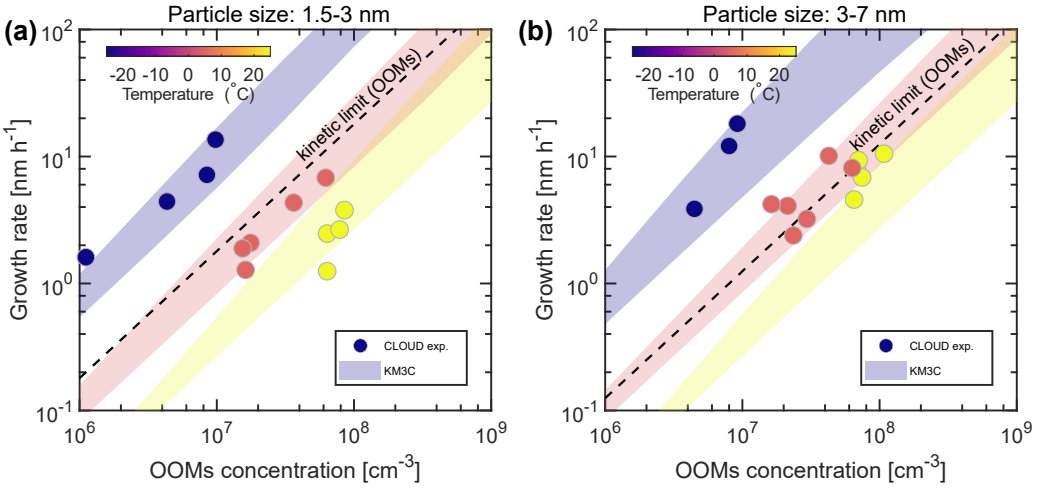

Figure 2. Secondary organic aerosol nanoparticle growth observed in laboratory experiments. Circular markers represent growth rates measured at different temperatures in the CERN CLOUD chamber (Stolzenburg et al., 2018, 2025) for particle size ranges of 1.5-3 nm **(a)** and 3-7 nm **(b)**. The dependence on temperature and concentration of oxygenated organic molecules (OOMs) determined by nitrate chemical ionization mass spectrometry (NO3-CIMS) was not captured by the modeling approach of Stolzenburg et al. (2025) (dashed line, "kinetic limit (OOMs)"). Considering also more volatile organic compounds detected by proton-transfer reaction time-of-flight mass spectrometry (PTR3, Stolzenburg et al. (2018)), volatility shifts according to the Clausius-Clapeyron equation, as well as variable particle-phase diffusivity, KM3C can reproduce both the temperature and concentration dependence (colored bands). The width of the colored bands corresponds to the same range of diffusivities as assumed in Fig. 1 (10^{-20} – 10^{-15} cm^2 s^{-1}, Sect. S5).

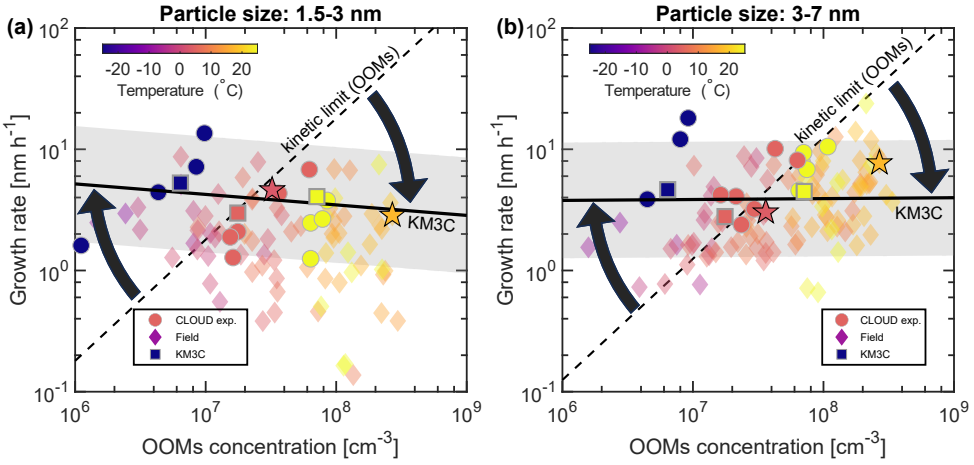

Figure 3. Range and buffering of observed and predicted atmospheric nanoparticle growth rates. Measurement data points color-coded by temperature represent growth rates as presented and discussed by Stolzenburg et al. (2025) for particles with diameters in the ranges of **(a)** 1.5-3 nm and **(b)** 3-7 nm, respectively. The data are plotted against the concentration of oxygenated organic molecules (OOMs) measured by NO3-CIMS during laboratory experiments in the CERN CLOUD chamber (circles, Stolzenburg et al., 2018) and during field measurements (diamonds) in Hyytiälä, Finland (Gonzalez Carracedo et al., 2022), Beijing, China (Qiao et al., 2021), and San Pietro di Capofiume, Italy (Cai et al., 2024). The two cases studied in Fig. 1 are highlighted with star-shaped markers. Square markers represent growth rates predicted by KM3C at the temperatures, median organic vapor concentrations and volatility distributions reported for the CERN CLOUD chamber experiments, and the solid black lines are linear fits to the model results. As indicated by the grey shaded areas, most of the growth rates observed in the field measurements and laboratory experiments fall within a factor of three relative to this line. The dashed black line is the kinetic limit reported by Stolzenburg et al. (2025), and the black arrows indicate the effective buffering of the organic vapor (OOMs) concentration dependence by temperature-related shifts in volatility and diffusivity.

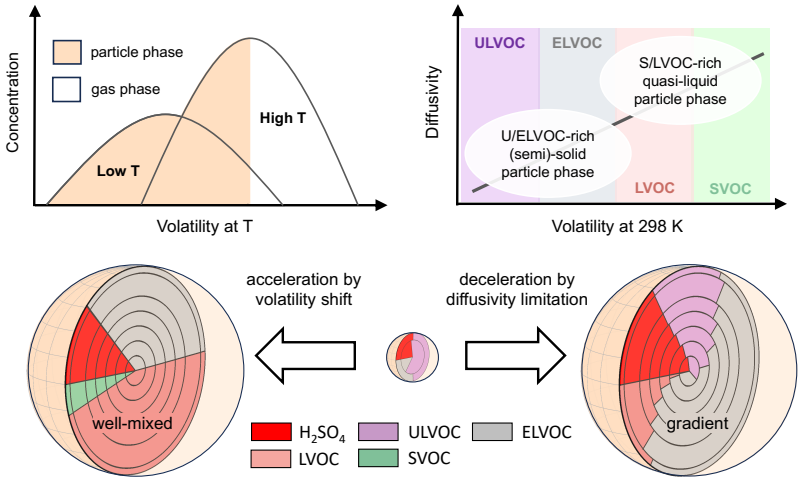

Figure 4. Key factors in the buffering of atmospheric nanoparticle growth rates. Ambient temperature influences the production and volatility distribution of condensable vapors in the atmosphere. An increase in temperature tends to enhance the production and concentration of organic vapors, but it also enhances their volatility (equilibrium vapor pressure) following the Clausius-Clapeyron equation and shifts the gas-particle partitioning towards the gas phase. These competing effects buffer the amount of vapors that are available to condense and drive particle growth. In addition, particle composition and phase state are influencing the molecular diffusivity, which tends to increase with increasing intrinsic volatility of the condensed organic compounds. At elevated temperatures, primarily very low volatile compounds (ULVOC, ELVOC) tend to condense and form (semi-)solid phases with kinetic limitations of diffusivity and surface-to-bulk transport, leading to differential concentration gradients and surface enrichment of more volatile compounds. At low temperatures, also more volatile compounds (SVOC, LVOC) tend to condense and favor the formation of quasi-liquid phases and well-mixed particles that are not subject to kinetic limitations by slow diffusion.

Supplement of

Buffering of atmospheric nanoparticle growth by temperature-dependent shifts in molecular composition, volatility and diffusivity

Zhiqiang Zhang[1], Hyun Gu Kang[1], Ulrich Pöschl[1], and Thomas Berkemeier[1]

[1]Multiphase Chemistry Department, Max Planck Institute for Chemistry, Hahn-Meitner-Weg 1, 55128 Mainz, Germany

Correspondence: Thomas Berkemeier (t.berkemeier@mpic.de)

Supplementary Text

S1 Kinetic multilayer model of multiphase chemistry

We use the kinetic multilayer model of multiphase chemistry (KM3C) to explicitly treat gas phase diffusion, particle-phase bulk diffusion, and multiphase partitioning kinetics based on vapor pressures (Fig. S9). KM3C is built in the framework of the kinetic multilayer meta model (KM-MEMO, Mishra et al., 2025), which is a Matlab toolkit that simplifies kinetic model construction by automatically generating and executing systems of differential equations from well-defined input files. KM3C addresses possible limitations in surface-bulk mass transfer and bulk diffusion, and detailed descriptions of the model and its predecessors are described elsewhere (Shiraiwa et al., 2012; Berkemeier et al., 2020; Kang et al., 2026). The model consists of the following compartments: gas phase, near-surface gas phase, a sorption layer, a quasi-static surface layer (near-surface bulk layer), and the particle bulk, subdivided into several bulk layers. The model is initiated with a freshly-nucleated particle (diameter of 0.9 nm) containing non-volatile organic species. When modeling the CERN CLOUD laboratory data, we fix the concentrations of gaseous OOMs to the values reported in Stolzenburg et al. (2018). When modeling the field measurement data, we interpolate the concentrations reported in Stolzenburg et al. (2025) of gaseous OOMs and H_2SO_4 across several time intervals.

In this study, we use a volatility basis set (VBS) approach that categorizes molecules by their saturation mass concentrations at 298 K (C^*_{298}) into logarithmically spaced volatility bins (Donahue et al., 2006, 2014; Stolzenburg et al., 2022). KM3C treats each volatility bin as a representative chemical species. For the field measurement data, we use average molecular weights reported for each volatility bin. For the CERN CLOUD chamber data, we use a linear relationship of volatility and molecular weight that we derive from the field measurements in a molecular corridor plot (Table S1 and Fig. S10, Shiraiwa et al., 2014). The model corrects C^*_{298} for temperature with the Clausius-Clapeyron equation (Eq. S1) and the enthalpy of vaporization

(ΔH_{vap}), where R is the gas constant. We calculate the ΔH_{vap} for each volatility bin using the empirical relationship between C^*_{298} and ΔH_{vap} (Eq. S2) proposed by Epstein et al. (2010) and use the parameters from Stolzenburg et al. (2022). An upper limit of 200 kJ mol^{-1} is applied to ΔH_{vap} (Cappa and Jimenez, 2010).

$$C^*(T) = C^*_{298} \times \exp\left(-\frac{\Delta H_{\text{vap}}}{R}\left(\frac{1}{T} - \frac{1}{298}\right)\right) \tag{S1}$$

$$\Delta H_{\text{vap}} = -5.7 \times \log_{10}(C^*_{298}) + 129 \tag{S2}$$

KM3C is sensitive to the bulk diffusion coefficient, which we vary across the range characteristic for liquid to solid phases. Nanoparticle growth is affected by lowered diffusivities in two ways: development of differential concentration gradients (i.e. different compounds exhibit concentration gradients of different strength and direction) and reduced surface-to-bulk transfer. Both lead to reduced condensation of relatively higher volatile compounds (SVOC, LVOC).

The model describes the temperature-dependence of bulk diffusivity with a similar Arrhenius-type equation (Eq. S3) and an activation energy of diffusion ($E_{\text{a,dif}}$). Here, we use a value of $E_{\text{a,dif}}$ = 40 kJ mol^{-1}, which is consistent with that of sucrose-water solutions (Kiland et al., 2019).

$$D_b(T) = D_{\text{b,298}} \times \exp\left(-\frac{E_{\text{a,dif}}}{R}\left(\frac{1}{T} - \frac{1}{298}\right)\right) \tag{S3}$$

We note that $E_{\text{a,dif}}$ will likely increase towards more viscous organic matrices, leading to super-Arrhenius behavior when approaching the glass transition, a property well-known from studies of the viscosity of so-called fragile glass-formers (Angell, 1991). Diffusion coefficients used in this study at different temperatures for simulating nanoparticle growth in field and CERN CLOUD chamber studies are listed in Table S2. A more detailed description of the composition- and temperature-dependence of the diffusion coefficient in organic nanoparticle growth can be found in Sects. S7 and S8 below.

Another process affecting nanoparticle growth is coagulation, which can increase measured growth rates (Cai et al., 2021, 2026). Coagulation was not explicitly treated in this study, as Stolzenburg et al. (2025) reported little influence of coagulation for the investigated field data, while Stolzenburg et al. (2018) included it into their uncertainty estimates for the investigated chamber data. Following Nguyen et al. (2026), we estimated the self-coagulation timescale (τ_{scoa}, Eq. S4) and show the results in Fig. S11.

$$\tau_{\text{scoa}} = \frac{2}{K N_{\text{p}}} \tag{S4}$$

where, N_{p} is the particle number concentration and K is the coagulation coefficient. We derive K from the formulas given in Nguyen et al. (2026) as a function of particle diameter, Brownian diffusivity, mean thermal velocity, and coagulation efficiency

(α). For details on the calculation of K, please refer to Table S1 in Nguyen et al. (2026). At a particle number concentration of 10^3 cm^{-3} (Stolzenburg et al., 2025), characteristic self-coagulation timescales (star-shaped markers) are much longer than the observation time of 6 hours (gray dashed line), irrespective of particle size (shadings) and coagulation efficiency (blue vs. black lines). Previous studies also suggested viscous particles might adopt a lower coagulation efficiency (Hou et al., 2020), which would further prolong the coagulation timescale. Besides self-coagulation, scavenging of nanoparticles by larger particles may occur, but these particles then simply do not contribute to nanoparticle growth rates measured by the appearance time method. Therefore, we assume a negligible impact of coagulation in this study. Moreover, the analysis and description of nanoparticle growth rates in atmospheric air masses can be influenced by differences between Lagrangian and Eulerian perspectives in the analysis and modeling of condensable vapor concentrations and aerosol particle size distributions. Such effects were not taken into account here but will be investigated in follow-up studies combining KM3C with regional and global 3D models of atmospheric transport and chemistry.

S2 Mass transfer coefficients

In KM3C, diffusion limitations affect growth rates mostly by slowing surface-to-bulk transfer, i.e. the transition of a molecule between being surface-adsorbed and being absorbed into the particle bulk. The surface-to-bulk transfer rate is directly proportional to the diffusivity in the topmost bulk layer and inversely proportional to the vapor pressure of the transported molecule (Shiraiwa et al., 2012; Berkemeier et al., 2020). Based on absorptive partitioning theory (Pankow, 1994), the surface-to-bulk transfer rate coefficient (k_{sb}) is calculated with Eq. S5:

$$k_{\mathrm{sb}} = \frac{2D_{\mathrm{b}}}{\delta_{\mathrm{s}} + \delta_{\mathrm{b1}}} \frac{k_{\mathrm{d}}}{k_{\mathrm{a}}} \frac{\sum [Y_i]_{\mathrm{b1}} RT}{p_{\mathrm{vap}} N_{\mathrm{A}}} \tag{S5}$$

in which, k_{d} and k_{a} are the desorption and adsorption rate coefficients. $\sum [Y]_{\mathrm{b1}}$ is the sum of the molecular concentrations of all species Y_i in the near-surface bulk layer. p_{vap} is the vapor pressure of the partitioning species, R is the gas constant, T is the temperature, and N_{A} is Avogadro's number. k_{bs} is the bulk-to-surface transfer rate coefficient and is calculated with Eq. S6, where D_{b} is the bulk diffusivity, δ_{s} is the depth of sorption layer, and δ_{b1} is the depth of the near-surface bulk layer.

$$k_{\mathrm{bs}} = \frac{2D_{\mathrm{b}}}{\delta_{\mathrm{s}} + \delta_{\mathrm{b1}}} \tag{S6}$$

We use a first-order adsorption rate coefficient (k_{a}, Eq. S7), where α and ω are the mass accommodation coefficient and the mean thermal velocity of the adsorbing molecule respectively. C_{g} and θ are the gas phase diffusion correction factor and the fractional surface coverage (Shiraiwa et al., 2012).

$$k_{\mathrm{a}} = C_{\mathrm{g}} \alpha \frac{\omega}{4} (1 - \theta) \tag{S7}$$

To obtain the total flow of adsorption F_{ads} (unit s^{-1}) of molecules to the particle surface, k_{a} is multiplied with the near-surface gas concentration [Z_{gs}] and the collision cross section A_{p} of the particle (Pöschl et al., 2007). This effective collision surface area of the particle in KM3C is calculated using the particle radius plus the sorption layer, for which we assume a thickness of 0.639 nm, corresponding to organic matter with an average molar mass of 220 g mol^{-1} and density of 1.4 g cm^{-3}.

The first-order desorption rate coefficient (k_{d}, Eq. S8) is the inverse of the surface desorption lifetime (τ_{d}), where A_{des} is the pre-exponential factor ($A_{\text{des}} = 10^{13}$) and E_{des} is the activation energy of desorption (Knopf et al., 2024). Using literature values, Knopf et al. (2024) found a relationship between the standard saturation vapor pressure $p_{\text{vap,298}}$ and E_{des}, which is shown in Fig. S12 and depends on the molecular oxygen-to-carbon ratio (O:C). As the organic compounds condensing on nanoparticles are likely highly oxygenated, we use a parameterization that runs along the left boundary of the data in this study. Note, however, that the choice of τ_{d} was not sensitive in the model simulations unless much larger values were chosen.

$$k_{\text{d}} = \frac{1}{\tau_{\text{d}}} = A_{\text{des}} \exp\left(\frac{-E_{\text{des}}}{RT}\right) \tag{S8}$$

The model corrects the vapor pressures for the Kelvin effect (Seinfeld and Pandis, 2016) by multiplying the vapor pressures with the Kelvin term ($K(D_{\text{p}})$, Eq. S9). Here, D_{p} is the diameter of the particle, and D_{K10} is the Kelvin diameter at which the curvature effect becomes important (Eq. S10).

$$K(D_{\text{p}}) = 10^{(D_{K10}/D_{\text{p}})} \tag{S9}$$

$$D_{K10}(T) = 4.8 \times (300 \times T^{-1}) \tag{S10}$$

In line with the results by Tröstl et al. (2016), we find the impact of the Kelvin term on the simulation results to be rather small.

S3 Adaptive layer resizing algorithm

KM3C adopts an adaptive layer resizing algorithm that dynamically splits layers when a layer grows too large and merges adjacent layers when they are too thin (Kang et al., 2026). This algorithm is able to account for concentration gradients dynamically as particles grow (or shrink) and can prevent numerical stiffness that arises when layers deplete. As the particles grow, solvating molecules enter the near-surface bulk layer, which can trigger a split of that layer via the adaptive layer resizing algorithm. However, this split can lead to an artificial and sudden increase in particle growth as k_{sb} and k_{bs} increase when δ_{b1} decreases. To solve this problem, we implement a moving-boundary algorithm (Couvidat and Sartelet, 2015; Kang et al., 2026), which keeps the depth of the near-surface bulk layer constant by increasing mass transport from the near-surface bulk layer to the underlying bulk layer when the the near-surface bulk layer grows. The enhanced diffusion is calculated based on the

molecular volume flow into the near-surface bulk layer. The near-surface bulk layer in KM3C adopts the role and properties of the quasi-static surface layer formalized and used in previous studies (Pöschl et al., 2007; Shiraiwa et al., 2012).

S4 Hyytiälä SMEAR II station field measurement data

Stolzenburg et al. (2025) reported field measurements of H_2SO_4, OOMs and nanoparticle growth at the SMEAR II station in the boreal forests of Hyytiälä, Finland from April 11th (3.8 °C, 50.7 % RH) and August 17th (17.5 °C, 49.9 % RH) of 2020 (Gonzalez Carracedo et al., 2022). The brown line and shadings in Fig. 1 in the main text shows the best estimate and uncertainty range of traditional model calculations. Shadings are obtained by shifting the volatility basis set by ± 1 bin. We use the same methodology for the uncertainty range of the KM3C model calculations. The authors also reported OOMs volatility distributions estimated using the identified molecular ion signals and a parameterization based on elemental ratios (Donahue et al., 2011). We use the reported ion masses for the molecular weights of the volatility bin species in KM3C (black and blue markers in Fig. S10).

S5 CERN CLOUD laboratory data

We use laboratory experimental data of dark α-pinene ozonolysis conducted at the Cosmics Leaving Outdoor Droplets (CLOUD) chamber at the European Organization for Nuclear Research (CERN) (Kirkby et al., 2011; Stolzenburg et al., 2018). Experiments were performed at three different temperatures (25, 5, and -25 °C). Proton transfer reaction (PTR3) and nitrate chemical ionization mass spectrometers (NO3-CIMS) were used to measure the gas-phase species. Stolzenburg et al. (2018) reported detailed organic vapor concentrations and volatility distributions for three experiments, which we digitized from the published Fig. 1 using WebPlotDigitizer. We simulate the experiments with KM3C at the temperatures reported and assuming $D_{b,298}$ = 10^{-18} cm^2 s^{-1}. The simulation results are displayed as square markers in Fig. 3 in the main text. Stolzenburg et al. (2018) did not report the specific ion masses, and we estimate the molecular weights for the products in the CLOUD experiments using the ion masses in Stolzenburg et al. (2025) (Table S1). These values are shown as the red circles in Figure S10. Colored bands in Fig. 2 in the main text are obtained by linearly scaling the condensable organic vapor concentrations in the model at the three respective temperatures (-25, 5, and 25°C) to obtain a series of model simulations at the same temperatures. In main text Fig. 2, we vary the bulk diffusion coefficient within the semi-solid phase state range (10^{-20} – 10^{-15} cm^2 s^{-1}) and scale with temperature to obtain the upper and lower boundaries of the colored bands.

The growth rates observed at high temperature in the CERN CLOUD chamber experiments of α-pinene ozonolysis under dark conditions (25°C, yellow bands and data points) are best reproduced assuming relatively low diffusivity for particles smaller than 3 nm (Fig. 2a in the main text) and higher diffusivity for larger nanoparticles (Fig. 2b in the main text). In contrast, reproducing the boreal summertime field observations requires low diffusivity for the entire size range up to 11 nm (Fig. 1a in the main text). These differences in diffusivity can be plausibly attributed to differences in particle composition and chemical aging. As shown in Fig. S2, smaller particles contain higher proportions of organic compounds with low intrinsic volatility

(ELVOC/ULVOC), while the uptake and partitioning of relatively more volatile compounds (SVOC/LVOC) tend to reduce the viscosity and increase the diffusivity of larger particles. Intrinsic volatility is often characterized by the saturation mass concentration at a standard temperature of 298 K (C^*_{298}, Schervish and Donahue, 2020; Donahue et al., 2026).

The molecular composition of SOA particles formed by dark ozonolysis of α-pinene (CERN CLOUD) is likely not the same as for particles formed in summertime boreal forest air (Hyytiälä), which may be influenced by other volatile precursors (monoterpenes, sesquiterpenes; Hellén et al., 2018) and photo-oxidants including OH radicals. Furthermore, sunlight and atmospheric photochemistry may promote condensed-phase reactions that can enhance the formation of more highly oxygenated compounds, dimers, oligomers, and other accretion products. Such condensed-phase reaction products with high molecular mass and low volatility can influence particle composition, viscosity, and diffusivity without being reflected in gas-phase measurements of condensable organic vapor concentrations and volatility distributions (Mehra et al., 2020; Maben and Ziemann, 2023; Kenseth et al., 2023; Kang et al., 2026). An accurate description of SOA nanoparticle growth may thus require resolution of molecular identities, their chemical evolution along molecular corridors, as well as matrix interactions influencing their physicochemical properties (Sect. S10; Shiraiwa et al., 2014; Li et al., 2016; Knopf et al., 2024).

To obtain shaded regions in main text Fig. 3, we scale the obtained growth rates by a factor of 3 to account for experimental uncertainties, possible differences in the ambient vapor composition compared to the CERN CLOUD measurements, and possible differences in particle phase state.

S6 Determination of nanoparticle growth rates

In both, KM3C used in this study and the two-film model used in Stolzenburg et al. (2025), the diameter growth rate of the particle (GR = $\mathrm{d}d_p/\mathrm{d}t$) was calculated from the $d_p(t)$ trajectory of a monodisperse particle population. The growth rate within a size interval is determined from the time required for a monodisperse particle to grow from one end of the size interval to the other:

$$GR_{1.5\text{–}3\,\mathrm{nm}} = \frac{\Delta d_p}{\Delta t_{1.5\text{–}3\,\mathrm{nm}}} = \frac{1.5\,\mathrm{nm}}{\Delta t_{1.5\text{–}3\,\mathrm{nm}}} \tag{S11}$$

$$GR_{3\text{–}7\,\mathrm{nm}} = \frac{\Delta d_p}{\Delta t_{3\text{–}7\,\mathrm{nm}}} = \frac{4\,\mathrm{nm}}{\Delta t_{3\text{–}7\,\mathrm{nm}}} \tag{S12}$$

For the CLOUD experiment, growth rate was estimated by the appearance-time method in the original study (Stolzenburg et al., 2018). In the Hyytiälä field measurements, growth rates were estimated with the appearance-time and maximum-concentration methods (Stolzenburg et al., 2023). Specifically, the maximum concentration method defines the representative time (t) as when the particle number concentration within a specific size bin peaks (Kulmala et al., 2013), typically determined by fitting a Gaussian function to each size channel's signal. The resulting time shift as a function of particle size reflects particle growth. The appearance time method uses the time (t_m) when the concentration reaches a specific percentage ($m\%$) of its maximum during an new particle formation event (Lehtipalo et al., 2014).

S7 Temperature-dependent diffusivity coefficients

The diffusivity in organic matter condensing at high temperature may be lower than in organic matter condensing at low temperature. For a certain gas-phase composition, this depends on the magnitudes of the enthalpies of vaporization and the activation energies of diffusion (Epstein et al., 2010; Kiland et al., 2019). The volatilities of organic compounds show Arrhenius-behavior following the Clausius-Clapeyron equation, but the viscosity of organic liquids approaching the glass transition generally exhibits super-Arrhenius behavior following the Vogel–Fulcher–Tammann equation (Bilde et al., 2015; Shiraiwa et al., 2017), which means that activation energies of diffusion are not constant over large temperature ranges. This interplay is important for determining whether a multiphase system of condensing vapors exhibits hardening or softening of the particle phase upon increase in temperature. In semi-solids, activation energies of diffusion may be smaller than enthalpies of vaporization, which would entail a hardening of organic aerosols towards higher temperatures. For glassy organics, however, activation energies of diffusion may be larger than enthalpies of vaporization and the dependence may reverse: a liquefaction of organic aerosols towards higher temperatures.

S8 Composition-dependent diffusivity coefficients

The diffusivity of a mixture of organic molecules depends on its chemical composition. We explore the implementation of parameterizations of bulk diffusivity (D_b) as function of saturation mass concentration (C^*) of different volatility bins. In the following, we present parameterizations developed by Li et al. (2020) (Sect. S8.1) and Kang et al. (2026) (Sect. S8.4). Afterwards, we explore the effects of plasticization by water (Sect. S8.2) and the size-dependence of aerosol phase state as suggested by Cheng et al. (2015) and investigated by Mahant et al. (2024) (Sect. S8.3).

S8.1 T_g-C^* parameterization by Li et al. (2020)

We calculate the glass transition temperature (T_g) of individual species i based on the parameterization proposed by Li et al. (2020):

$$T_{g,i} = 288.70 - 15.33 \times \log_{10}(C^*_{298}) - 0.33 \times \log_{10}(C^*_{298}) \tag{S13}$$

The glass transition temperature of the mixture within layer l is calculated from the $T_{\mathrm{g},i}$ of the individual species, weighted with their mass fraction ($w_{i,l}$) in that layer.

$$T_{\mathrm{g},l} = \sum_i w_{i,l} T_{\mathrm{g},i} \tag{S14}$$

As the T_g of sulfate, we assume the value measured by ammonium bisulfate of 220 K (Dette and Koop, 2015). The viscosity (η_l) of mixture in layer l can be calculated from the average $T_{\mathrm{g},l}$ with the Vogel–Fulcher–Tammann (VFT) equation.

$$T_{0,l} = \frac{39.17 \times T_{\mathrm{g},l}}{D + 39.17} \tag{S15}$$

$$\eta_l = \eta_\infty e^{\frac{T_{0,l} D}{T - T_{0,l}}} \tag{S16}$$

where η_∞ is the viscosity at infinite temperature (10^{-5} Pa s; Angell (1991)). $T_{0,l}$ is the Vogel temperature, which was derived assuming η_l = 10^{12} Pa s when T = $T_{\mathrm{g},l}$. For T < $T_{\mathrm{g},l}$, η_l is capped at 10^{12} Pa s. D is the fragility parameter, which is assumed to be 10 here. T is the temperature.

From the glass transition temperature and viscosity of the mixture, we calculate molecular diffusivities in layer l based on the Stokes-Einstein relation (Koop et al., 2011).

$$D_{\mathrm{b},l} = \frac{kT}{6\pi r_l \eta_l} \tag{S17}$$

Here, k is the Boltzmann constant. r_l is the radius of the diffusing species in layer l, which is the average effective molecular length of all species.

S8.2 Plasticization of water as a function of relative humidity

T_{g} of organics (H_2SO_4)-water mixtures at given RH can be estimated using the Gordon-Taylor equation (Gordon and Taylor, 1952).

$$T_{\mathrm{g},l}(w_{\mathrm{org},l}) = \frac{(1 - w_{\mathrm{org},l}) T_{g,\mathrm{w}} + \frac{1}{k_{\mathrm{GT}}} w_{\mathrm{org},l} T_{\mathrm{g},l}}{(1 - w_{\mathrm{org},l}) + \frac{1}{k_{\mathrm{GT}}} w_{\mathrm{org},l}} \tag{S18}$$

where $w_{\mathrm{org},l}$ is the mass fraction of organics and H_2SO_4 in layer l. $T_{g,\mathrm{w}}$ is the glass transition temperature of water (136 K). k_{GT} is the Gordon-Taylor constant (2.5). We calculate the mass fraction of water with Raoult's law and the effective hygroscopicity parameter (κ; Petters and Kreidenweis (2007)), and then $T_{\mathrm{g},l}(w_{\mathrm{org},l})$ of organics (H_2SO_4)-water mixtures in layer l is used in Eq. S15 and the following calculations.

In the effective hygroscopicity parameter method, the mass concentrations of water absorbed by nanoparticles can be estimated as:

$$m_{\mathrm{H_2O},l} = \frac{\kappa \rho_{\mathrm{w}} m_{\mathrm{SOA},l}}{\rho_{\mathrm{SOA}} \left(\frac{1}{a_{\mathrm{w}}} - 1 \right)} \tag{S19}$$

where ρ_{w} and ρ_{SOA} are the densities of water (1 g cm^{-3}) and organics (1.4 g cm^{-3}), respectively. $m_{\mathrm{SOA},l}$ is the mass concentration of organics in layer l. a_{w} is the water activity calculated as a_{w} = RH/100.

$w_{\text{org},l}$ can then be calculated and used in Eq. S18 as:

$$w_{\text{org},l} = \frac{m_{\text{SOA},l}}{m_{\text{SOA},l} + m_{\text{H}_2\text{O},l}} \tag{S20}$$

In the Raoult's law method, the mole fraction of water in layer l at the particle size of D_{p} can calculated as:

$$x_{\text{w},l} = \frac{RH}{100 \times K(D_{\text{p}})} \tag{S21}$$

where $K(D_{\text{p}})$ is the Kelvin term at particle size of D_{p}, and can be calculated in Eq. S9. $w_{\text{org},l}$ can then be calculated and used in Eq. S18 as:

$$w_{\text{org},l} = \frac{(1 - x_{\text{w},l}) \times M_{SOA}}{x_{\text{w},l} \times M_{\text{w}} + (1 - x_{\text{w},l}) \times M_{\text{SOA}}} \tag{S22}$$

where M_{SOA} is the molar mass of organics (250 g mol^{-1}) for simplification. M_{w} is the molar mass of water (18 g mol^{-1}).

S8.3 Particle size effects on phase state

Influence of particle size (d_{p}) on phase transition (T_{g}) is accounted for followed by Mahant et al. (2024) as detailed in Figure S6. ΔT_{g} is the depression of glass transition temperature relative to average T_{g} of the mixture in each layer, which is then accounted for in $T_{0,l}$ and the following calculations.

$$\log_{10}(\Delta T_g) = 1.83 - 10^{(0.43 \times (\log_{10}(d_p) - 2.37))} \tag{S23}$$

$$T_{0,l} = \frac{39.17 \times (T_{\text{g},l} - \Delta T_{\text{g}})}{D + 39.17} \tag{S24}$$

S8.4 D_{b}-C^* parameterization by Kang et al. (2026)

Following Kang et al. (2026), we express the dependence of self-diffusivity of each species ($D_{\text{b,298}}$) on the effective saturation mass concentration at 298 K (C^*_{298}) in a log-log relationship.

$$\log_{10}(D_{\text{b,298}}) = 0.761 \times \log_{10}(C^*_{298}) - 14.9 \tag{S25}$$

The diffusivity in each layer ($D_{\text{b,298},l}$) is calculated with the Vignes equation (Vignes, 1966), which is a logarithmic mixing rule and weights $D_{\text{b,298}}$ of each species i by its mass fraction w in layer l ($w_{i,l}$). Non-volatile species are assumed to adopt the

same $D_{b,298}$ as the species in the lowest volatility bin. To have H_2SO_4 act as plasticizer, we use a high $D_{b,298}$ of 10^{-12} cm^2 s^{-1}.

$$D_{b,298,l} = \prod_i (D_{b,298,i})^{w_{i,l}} \tag{S26}$$

In line with the upper limit of viscosity in Li et al. (2016), Kang et al. (2026) use a lower limit of $D_{b,298,l}$ of 10^{-20} cm^2 s^{-1}. An implementation of the particle size effect is not available for the $D_b - C^*$ parameterization at this moment and will be the topic of future studies.

S9 Model simulations with composition-dependent diffusion coefficients

Inserting the diffusivity parameterizations described in Sect. S8 above into KM3C, we can calculate diffusivities for each particle layer as a function of chemical composition and time (Kang et al., 2026).

As detailed in Fig. S4, the model simulations following Li et al. (2020) predict glassy solid nanoparticle phase states with glass transition temperatures (T_g) well above 300 K and diffusivities smaller than 10^{-20} cm^2 s^{-1} throughout the investigated growth events in summer and spring. Plasticizer effects of water and sulfate were taken into account (Sect. S8; Koop et al., 2011; Dette and Koop, 2015), but did not alter the modeling results substantially.

The model simulations following Kang et al. (2026) in Fig. S5 predict time-dependent and radially inhomogenous semi-solid phase states with diffusivities that are initially lower in summer than in spring, and of comparable magnitude overall (10^{-20} to 10^{-18} cm^2 s^{-1}). In both scenarios, the diffusivity increases over time as the particles grow by condensation of relatively more volatile compounds (Figs. S4, S5).

To explore the potential influence of nanosize effects following Cheng et al. (2015), we combined the parameterization of Li et al. (2020) with data measured by Mahant et al. (2024) and find that glass transition temperatures decrease substantially ($\Delta T_g \sim 40 - 50$ K), but not below 300 K. As the nanoparticle size effect declines towards larger particle sizes (Fig. S6), condensation of higher volatile vapors offsets this change, leading to a near-constant T_g around 320 K. In contrast, Virtanen et al. (2010) and Virtanen et al. (2011) found an amorphous solid phase state for Finnish boreal forest aerosol particles. They reported that particle bounce decreased at the smallest diameters they investigated (17-30 nm), suggesting that these particles may not have been glassy. Thus, the relations between nanoparticle growth, phase state, and bounce as well as additional effects such as enhanced mobility in the surface layers of solid particles (quasi-liquid layers) warrant further investigation in follow-up studies (McNeill et al., 2006; Stevenson and Wolynes, 2008; Tian et al., 2022).

S10 Volatility basis sets vs. molecular resolution

Our model currently assigns identical self-diffusion coefficients to the many different organic compounds lumped into each bin of the applied decadic volatility basis sets (VBS). We note, however, that molecules in the same VBS bin may exhibit

different properties such as diffusivity and desorption lifetime based on their molecular structure and functionalities, even if they exhibit similar intrinsic volatilities. Furthermore, the properties of organic aerosol mixtures may deviate from linear combinations of individual species properties. Fully resolving SOA nanoparticle growth may thus require a detailed accounting of matrix interactions, molecular identities and molecular corridors along which the gas-phase and condensed-phase composition of organic aerosols evolve (Shiraiwa et al., 2014; Li et al., 2016; Knopf et al., 2024).

Supplementary Figures

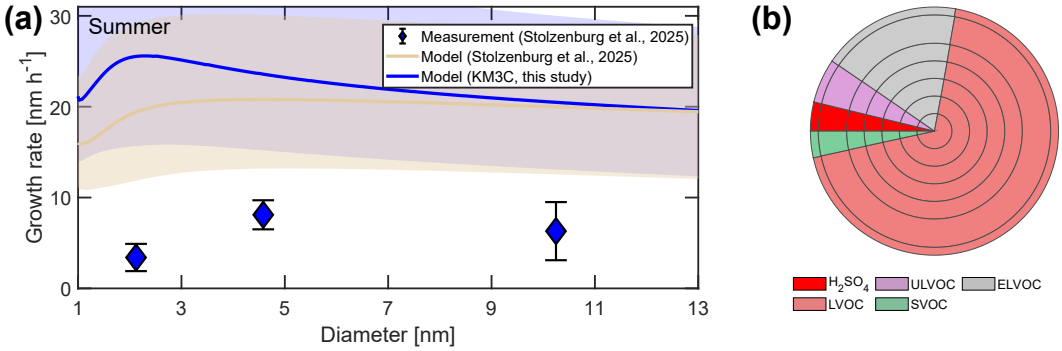

Figure S1. Observed and modelled atmospheric nanoparticle growth rates in a field experiment (Hyytiälä, 17th August, 2020). Same as Figs. 1a,c, but a higher diffusivity ($D_{\mathrm{b},298} = 10^{-15}$ cm^2 s^{-1}) is utilized in KM3C modeling. **(a)** Observed growth rates (blue diamond markers and error bars representing arithmetic mean values and standard deviations) and vapor concentration-based predictions obtained with a two-film model (Stolzenburg et al., 2025, brown line and shading for best estimate and uncertainty range by shifting full VBS by $\pm$ 1 bin). The new multiphase kinetic model (KM3C; blue line and shading for best estimate and uncertainty range by shifting full VBS by $\pm$ 1 bin) predicts similar growth rates to Stolzenburg et al. (2025) but also overestimates the observed growth rates. **(b)** Higher diffusivity ($D_{\mathrm{b},298} = 10^{-15}$ cm^2 s^{-1}) leads to well-mixed particles.

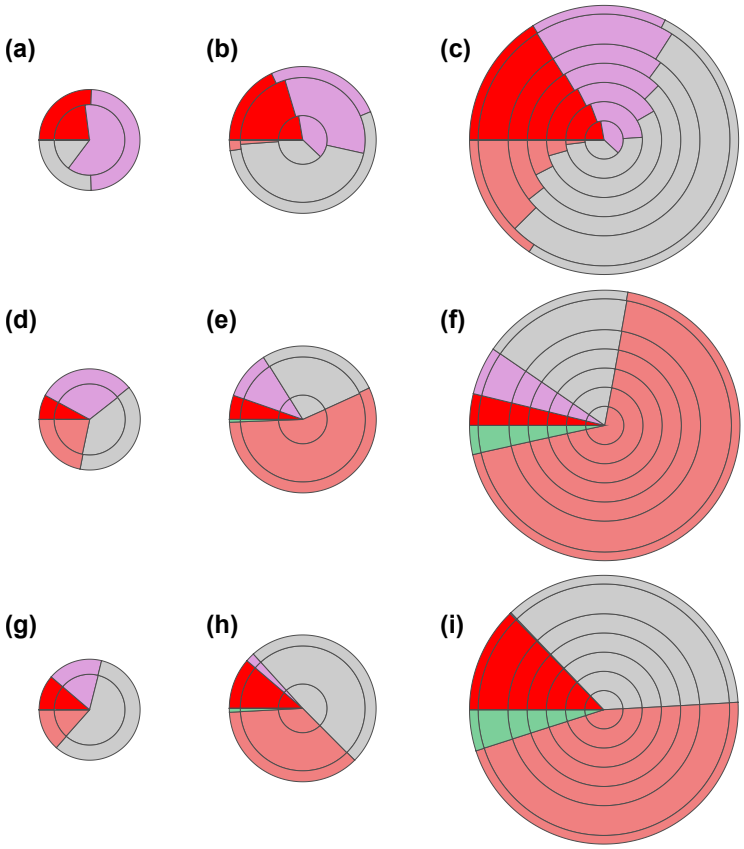

Figure S2. Radial concentration profiles for nanoparticles at diameters of 1.5 nm, 3 nm, and 7 nm for **(a-c)** the summer case with lower diffusivity ($D_{\mathrm{b},298}$ = 10^{-20} cm^2 s^{-1}), **(d-f)** the summer case with higher diffusivity ($D_{\mathrm{b},298}$ = 10^{-15} cm^2 s^{-1}) and **(g-i)** the spring case with higher diffusivity ($D_{\mathrm{b},298}$ = 10^{-15} cm^2 s^{-1}), respectively. The analysis shows that the particle core largely retains the initial composition dominated by relatively less volatile vapors (ELVOC, ULVOC) when diffusivity is low (panels a-c). In a sensitivity test with high diffusivity and otherwise unchanged conditions, relatively more volatile vapors (SVOC, LVOC) are readily taken up and well-mixed throughout the particle (panels d-f).

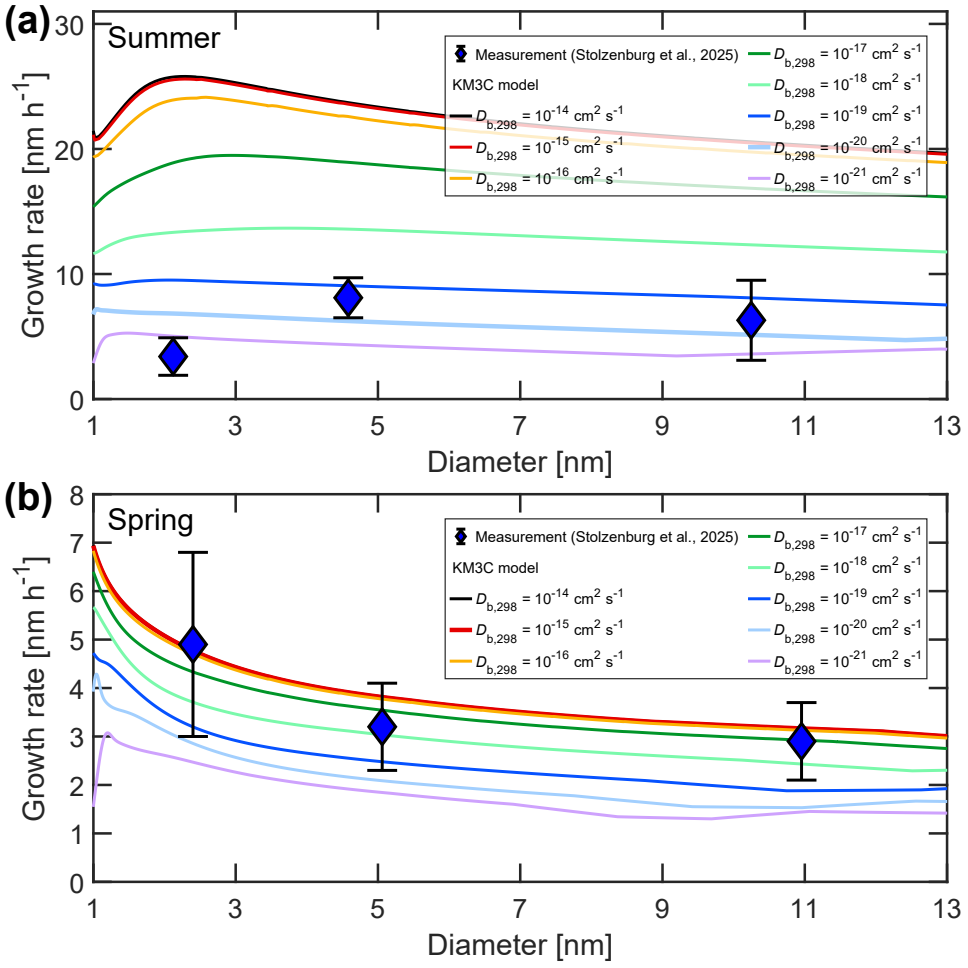

Figure S3. Observed (blue diamond markers and error bars) and KM3C-modelled (solid lines) atmospheric nanoparticle growth rates at a boreal forest site (Hyytiälä, Finland) in **(a)** summer and **(b)** spring, respectively. A range of diffusivities ($D_{b,298} = 10^{-21} - 10^{-14}$ cm^2 s^{-1}) shown with different colors is utilized in KM3C simulations.

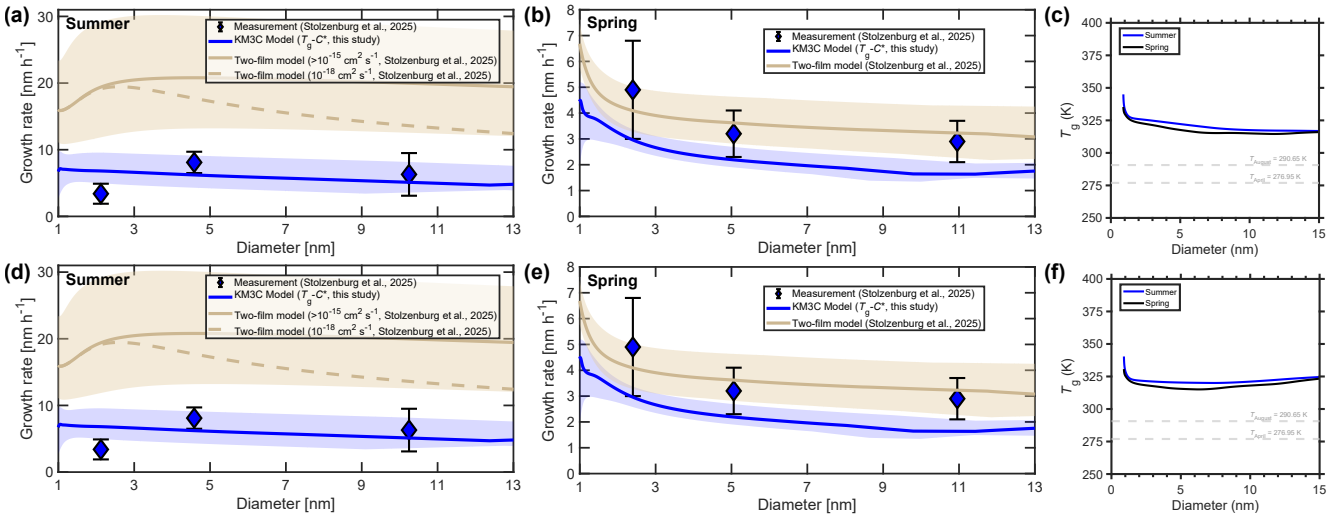

Figure S4. Observed (blue diamond markers and error bars) and modelled atmospheric nanoparticle growth rates in field experiments (Hyytiälä, Finland) in summer **(a, d)** and spring **(b, e)**, respectively. Brown line and shading represent a two-film model (Stolzenburg et al., 2025). Blue line and shading represent the KM3C model in which diffusivity is estimated following Li et al. (2020). Panels **(c)** and **(f)** show the predicted average glass transition temperature (T_g) as a function of particle size. In all the simulations shown here, T_g depression as a function of nanoparticle size following Mahant et al. (2024) is considered. In panels **(a-c)**, the water content of the SOA-H_2SO_4-water mixture is calculated using Raoult's law. In panels **(d-f)**, the water content of the mixture is calculated using an effective hygroscopicity parameter κ of approximately 0.01 as reported by Mikhailov et al. (2013) for the hygroscopic growth of ambient SOA under subsaturated conditions (RH $\sim$ 50%).

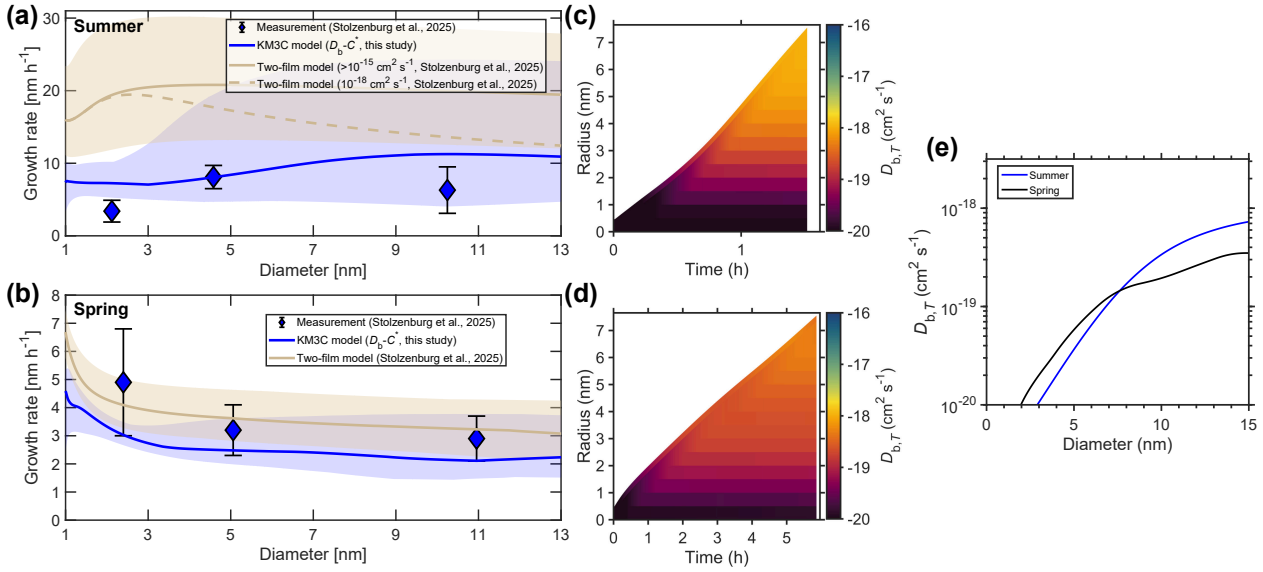

Figure S5. Observed (blue diamond markers and error bars) and modelled atmospheric nanoparticle growth rates in field experiments (Hyytiälä, Finland) in **(a)** summer and **(b)** spring, respectively. Brown line and shading represent a two-film model (Stolzenburg et al., 2025). Blue line and shading represent the KM3C model in which diffusivity is estimated following Kang et al. (2026). Panels **(c)** and **(d)** show the radial profiles of diffusivity as a function of time in summer and spring, respectively. Panel **(e)** shows the predicted diffusivity as a function of particle size using the average particle composition.

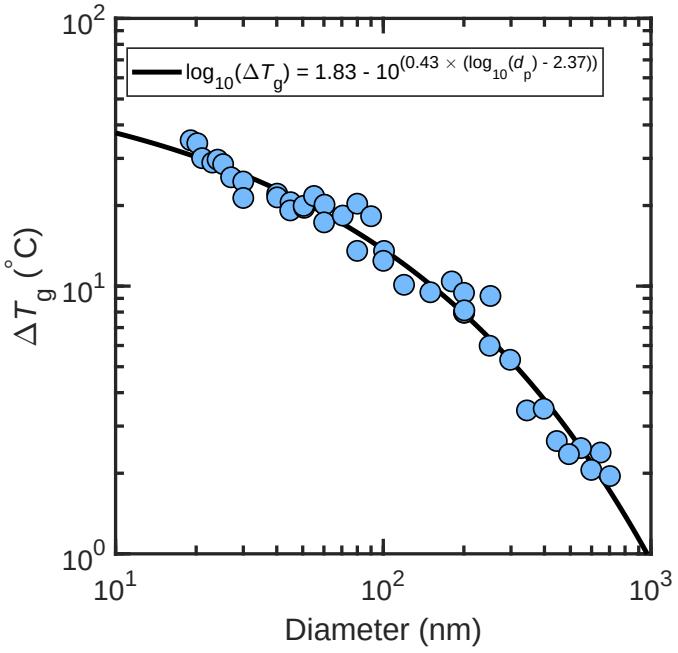

Figure S6. Glass transition temperature depression as a function of nanoparticle diameter. The black solid line represents fitting an exponential function to experimental data (blue circular markers) digitized from Mahant et al. (2024).

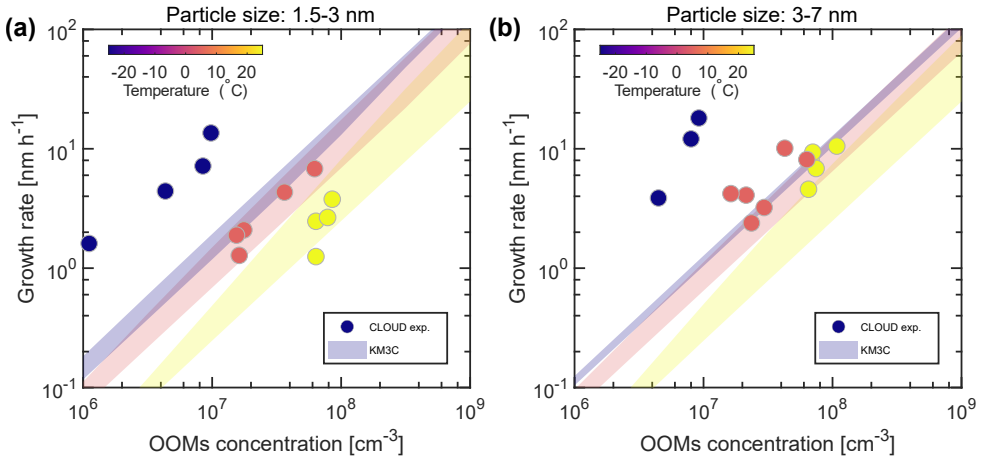

Figure S7. Nanoparticle growth rates in laboratory chamber experiments in the CERN CLOUD chamber and simulated with the KM3C kinetic model. Same as Fig. 2, but KM3C (colored bands) simulates nanoparticle growth rates for **(a)** 1.5-3 nm and **(b)** 3-7 nm using only the concentration of OOMs measured by NO3-CIMS data provided in Stolzenburg et al. (2018). Colored bands are obtained by linearly scaling the condensable organic material concentrations in the model at the three respective temperatures (-25, 5 and 25°C). Upper and lower boundaries of the shaded areas are obtained by varying the bulk diffusion coefficient $D_{b,298}$ within 10^{-20} – 10^{-15} cm^2 s^{-1} and detailed in Sect. S5.

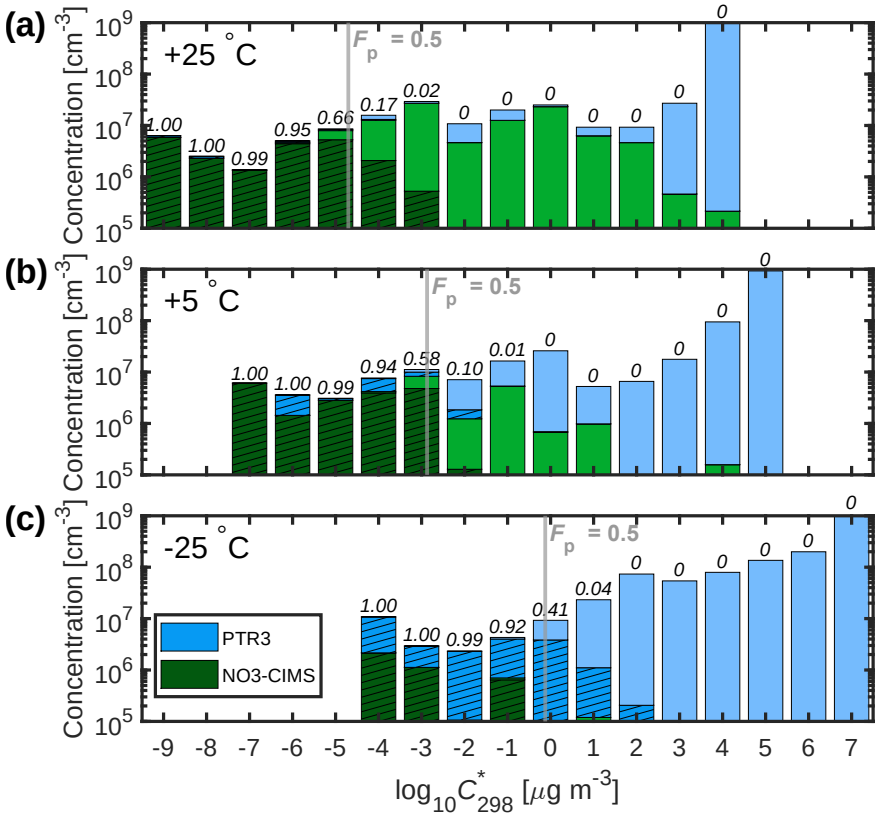

Figure S8. Volatility distributions of three experiments in the CERN CLOUD chamber. Experiments were conducted at **(a)** 25 °C, **(b)** 5 °C and **(c)** -25 °C reported by Stolzenburg et al. (2018). Data were digitized from the published Fig. 1 in Stolzenburg et al. (2018) using WebPlotDigitizer. Shaded areas and numbers above the bars indicate fractions that partition into the particle phase (F_p) at an aerosol mass loading of 2×10^{-5} µg m^{-3} assuming equilibrium partitioning in a closed system (Pankow, 1994), corresponding to 10^3 particles cm^{-3} with 3 nm diameter, and the grey vertical lines indicate the volatility where F_p = 0.5.

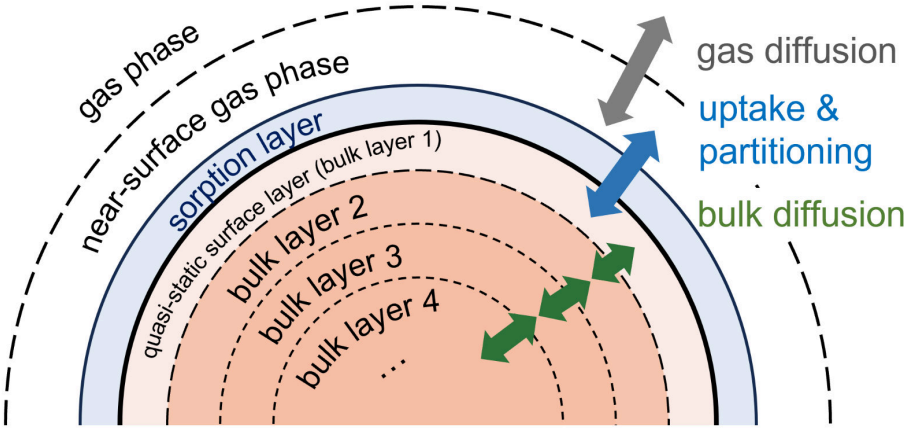

Figure S9. Overview of the kinetic multilayer model of multiphase chemistry (KM3C) used in this study. The particle bulk is subdivided into model layers to form concentration gradients and address slow diffusion.

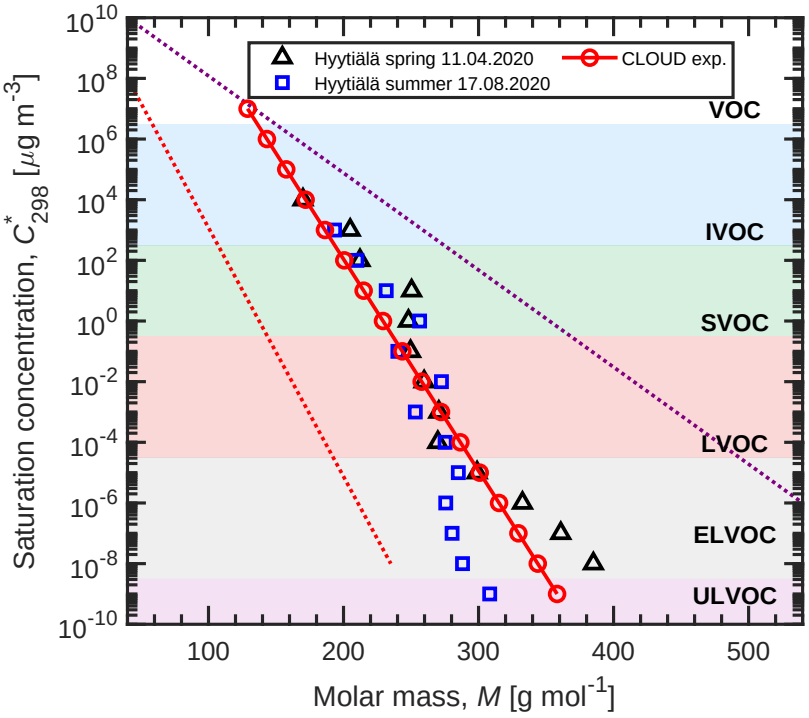

Figure S10. Molecular corridors of SOA evolution. KM3C incorporates volatility (298 K) and molar mass data from the field measurements in Hyytiälä, Finland, 11th April, 2020 (black triangles) and 17th August, 2020 (blue squares) in Stolzenburg et al. (2025). A linear relationship derived from these field measurements is applied to the CERN CLOUD chamber simulations (red circles).

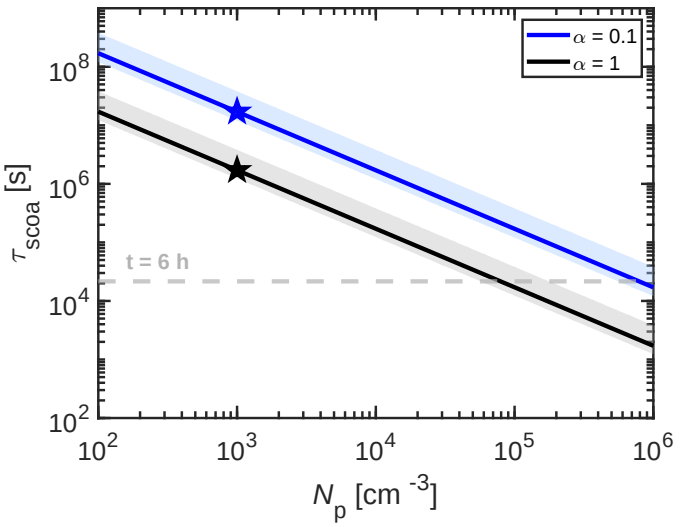

Figure S11. Characteristic self-coagulation timescale for monodisperse particles as a function of different particle number concentrations ($N_p = 10^2$ - 10^6 cm^{-3}) at 5 nm (solid lines) and for the range of 1-10 nm (shadings), where the upper bound corresponds to 1 nm and the lower bound to 10 nm. Calculations were performed for coagulation efficiencies (α) of 0.1 (blue) and 1 (black). The star-shaped markers indicate a nanoparticle concentration level of 10^3 cm^{-3} as indicated by Stolzenburg et al. (2025) (DOI: 10.48436/9633r-zf904).

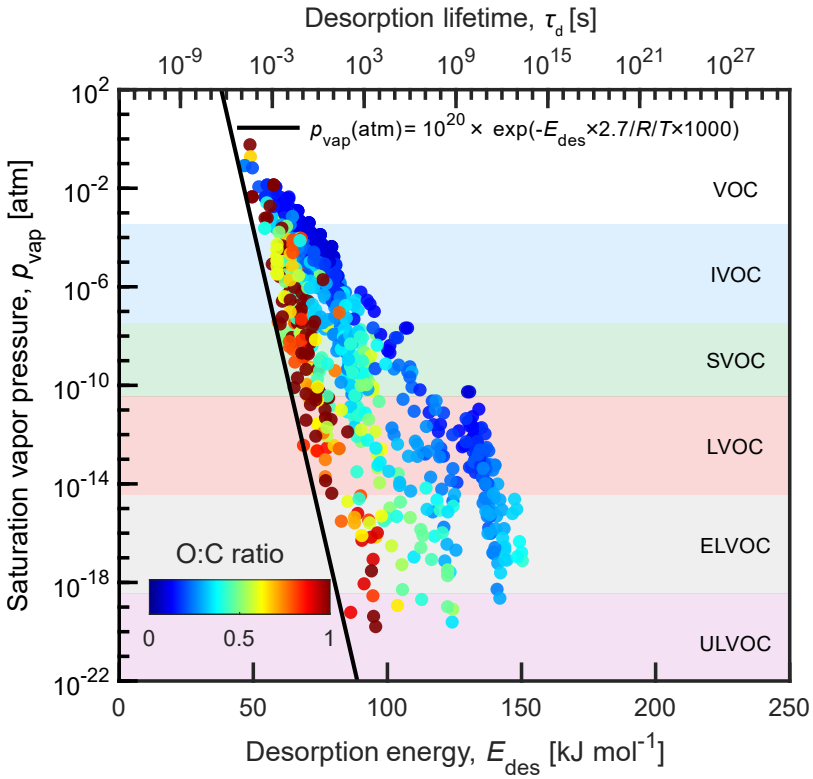

Figure S12. Relationship between saturation vapor pressure (p_{vap} at 298 K), desorption energies (E_{des}) implemented in KM3C. Desorption lifetime (τ_d) of species with a molar mass of 220 g mol^{-1} at 298 K is shown on the top axis. Markers indicate literature data (Knopf et al., 2024), where the colors show the O:C of the molecules. The black line is drawn using the shown equation, which is the parameterization used to retrieve E_{des} in KM3C.

Supplementary Tables

Table S1. Species measured in field measurements at a boreal forest site (Hyytiälä, Finland, 11 April and 17 August 2020) and in laboratory experiments (CERN CLOUD chamber), along with the volatility at 298 K and molar mass for each species used in KM3C in this study.

Species	Molar mass (Summer, g mol^{-1})	Molar mass (Spring, g mol^{-1})	Molar mass (CLOUD exp., g mol^{-1})
SOA (C^* = 10^7 µg m^{-3})	-	-	129
SOA (C^* = 10^6 µg m^{-3})	-	-	143
SOA (C^* = 10^5 µg m^{-3})	-	-	158
SOA (C^* = 10^4 µg m^{-3})	-	170	172
SOA (C^* = 10^3 µg m^{-3})	193	205	186
SOA (C^* = 10^2 µg m^{-3})	210	212	201
SOA (C^* = 10^1 µg m^{-3})	232	250	215
SOA (C^* = 10^0 µg m^{-3})	256	248	229
SOA (C^* = 10^{-1} µg m^{-3})	240	250	244
SOA (C^* = 10^{-2} µg m^{-3})	273	260	258
SOA (C^* = 10^{-3} µg m^{-3})	253	271	272
SOA (C^* = 10^{-4} µg m^{-3})	275	270	287
SOA (C^* = 10^{-5} µg m^{-3})	285	299	301
SOA (C^* = 10^{-6} µg m^{-3})	276	333	315
SOA (C^* = 10^{-7} µg m^{-3})	280	361	330
SOA (C^* = 10^{-8} µg m^{-3})	288	385	344
SOA (C^* = 10^{-9} µg m^{-3})	308	-	358
SOA (non-volatile) [a]	308	385	358
H_2SO_4 [b]	98	98	-

[a] Species in pre-existing nanoparticles are assumed to be non-volatile and are grouped into ULVOC in this study, and the molar mass of them are assumed to be the same as species in the lowest volatility bin.

[b] H_2SO_4 is assumed to have negligible vapor pressure following the assumption in the previous literature (Nieminen et al., 2010; Häkkinen et al., 2013).

Table S2. Diffusion coefficients used in this study at different temperatures for simulating nanoparticle growth in field and CERN CLOUD chamber studies.

	T (°C)	$D_{\mathrm{b},T}$ ($\mathrm{cm^2\,s^{-1}}$)		
		$D_{\mathrm{b},298} = 1 \times 10^{-15}$ ($\mathrm{cm^2\,s^{-1}}$)	$D_{\mathrm{b},298} = 1 \times 10^{-18}$ ($\mathrm{cm^2\,s^{-1}}$)	$D_{\mathrm{b},298} = 1 \times 10^{-20}$ ($\mathrm{cm^2\,s^{-1}}$)
Field	17.5 (summer)	-	6.59×10^{-19}	6.59×10^{-21}
	3.8 (spring)	2.91×10^{-16}	2.91×10^{-19}	-
CERN CLOUD chamber	-25	3.87×10^{-17}	3.87×10^{-20}	3.87×10^{-22}
	5	3.13×10^{-16}	3.13×10^{-19}	3.13×10^{-21}
	25	1×10^{-15}	1×10^{-18}	1×10^{-20}

References

Angell, C.: Relaxation in liquids, polymers and plastic crystals — strong/fragile patterns and problems, J. Non-Cryst. Solids, 131-133, 13–31, https://doi.org/https://doi.org/10.1016/0022-3093(91)90266-9, 1991.

Berkemeier, T., Takeuchi, M., Eris, G., and Ng, N. L.: Kinetic modeling of formation and evaporation of secondary organic aerosol from NO_3 oxidation of pure and mixed monoterpenes, Atmos. Chem. Phys., 20, 15 513–15 535, https://doi.org/10.5194/acp-20-15513-2020, 2020.

Bilde, M., Barsanti, K., Booth, M., Cappa, C. D., Donahue, N. M., Emanuelsson, E. U., McFiggans, G., Krieger, U. K., Marcolli, C., Topping, D., Ziemann, P., Barley, M., Clegg, S., Dennis-Smither, B., Hallquist, M., Hallquist, M., Khlystov, A., Kulmala, M., Mogensen, D., Percival, C. J., Pope, F., Reid, J. P., Ribeiro da Silva, M. A. V., Rosenoern, T., Salo, K., Soonsin, V. P., Yli-Juuti, T., Prisle, N. L., Pagels, J., Rarey, J., Zardini, A. A., and Riipinen, I.: Saturation Vapor Pressures and Transition Enthalpies of Low-Volatility Organic Molecules of Atmospheric Relevance: From Dicarboxylic Acids to Complex Mixtures, Chem. Rev., 115, 4115–4156, https://doi.org/10.1021/cr5005502, 2015.

Cai, R., Li, C., He, X.-C., Deng, C., Lu, Y., Yin, R., Yan, C., Wang, L., Jiang, J., Kulmala, M., and Kangasluoma, J.: Impacts of coagulation on the appearance time method for new particle growth rate evaluation and their corrections, Atmos. Chem. Phys., 21, 2287–2304, https://doi.org/10.5194/acp-21-2287-2021, 2021.

Cai, R., Li, X., Li, Y., Blichner, S., Stolzenburg, D., Zha, Q., Cai, J., Nie, W., Yan, C., Huang, D. D., Wang, Z., Wu, J., Yin, R., Sarnela, N., Huang, W., Tuovinen, S., Holm, S., Ahonen, L., Yao, L., Ding, A., Bianchi, F., Liu, Y., Winkler, P. M., Petäjä, T., Chen, J., Kerminen, V.-M., Wang, L., Worsnop, D., Jiang, J., Kulmala, M., and Kangasluoma, J.: The key role of nanoparticle concentration gradient in aerosol initial growth, Nat. Commun., https://doi.org/10.1038/s41467-026-70082-2, 2026.

Cappa, C. D. and Jimenez, J. L.: Quantitative estimates of the volatility of ambient organic aerosol, Atmos. Chem. Phys., 10, 5409–5424, https://doi.org/10.5194/acp-10-5409-2010, 2010.

Cheng, Y., Su, H., Koop, T., Mikhailov, E., and Pöschl, U.: Size dependence of phase transitions in aerosol nanoparticles, Nat. Commun., 6, 5923, https://doi.org/10.1038/ncomms6923, 2015.

Couvidat, F. and Sartelet, K.: The Secondary Organic Aerosol Processor (SOAP v1.0) model: a unified model with different ranges of complexity based on the molecular surrogate approach, Geosci. Model Dev., 8, 1111–1138, https://doi.org/10.5194/gmd-8-1111-2015, 2015.

Dette, H. P. and Koop, T.: Glass Formation Processes in Mixed Inorganic/Organic Aerosol Particles, J. Phys. Chem. A, 119, 4552–4561, https://doi.org/10.1021/jp5106967, 2015.

Donahue, N. M., Robinson, A. L., Stanier, C. O., and Pandis, S. N.: Coupled Partitioning, Dilution, and Chemical Aging of Semivolatile Organics, Environ. Sci. Technol., 40, 2635–2643, https://doi.org/10.1021/es052297c, 2006.

Donahue, N. M., Epstein, S. A., Pandis, S. N., and Robinson, A. L.: A two-dimensional volatility basis set: 1. organic-aerosol mixing thermodynamics, Atmos. Chem. Phys., 11, 3303–3318, https://doi.org/10.5194/acp-11-3303-2011, 2011.

Donahue, N. M., Robinson, A. L., Trump, E. R., Riipinen, I., and Kroll, J. H.: Volatility and Aging of Atmospheric Organic Aerosol, in: Atmospheric and Aerosol Chemistry, edited by McNeill, V. F. and Ariya, P. A., Topics in Current Chemistry, pp. 97–143, Springer, Berlin, Heidelberg, https://doi.org/10.1007/128_2012_355, 2014.

Donahue, N. M., Dada, L., Stolzenburg, D., Sommer, E., Simon, M., Schervish, M., DeVivo, J., Stinchfield, A., Burton, N., Bhattacharyya, N., Lopez, B., Wang, M., Scholz, W., Almeida, J., Zhao, B., Heinritzi, M., Gordon, H., Hansel, A., Curtius, J., Lehtipalo, K., El Haddad,

I., Kirkby, J., Flagan, R., Kulmala, M., and Worsnop, D.: On describing particle nucleation within the Volatility Basis Set, Atmos. Chem. Phys., 26, 8311–8339, https://doi.org/10.5194/acp-26-8311-2026, 2026.

Epstein, S. A., Riipinen, I., and Donahue, N. M.: A Semiempirical Correlation between Enthalpy of Vaporization and Saturation Concentration for Organic Aerosol, Environ. Sci. Technol., 44, 743–748, https://doi.org/10.1021/es902497z, pMID: 20025284, 2010.

Gonzalez Carracedo, L., Lehtipalo, K., Ahonen, L. R., Sarnela, N., Holm, S., Kangasluoma, J., Kulmala, M., Winkler, P. M., and Stolzenburg, D.: On the relation between apparent ion and total particle growth rates in the boreal forest and related chamber experiments, Atmos. Chem. Phys., 22, 13 153–13 166, https://doi.org/10.5194/acp-22-13153-2022, 2022.

Gordon, M. and Taylor, J. S.: Ideal copolymers and the second-order transitions of synthetic rubbers. i. non-crystalline copolymers, J. Appl. Chem., 2, 493–500, https://doi.org/10.1002/jctb.5010020901, 1952.

Häkkinen, S. A. K., Manninen, H. E., Yli-Juuti, T., Merikanto, J., Kajos, M. K., Nieminen, T., D'Andrea, S. D., Asmi, A., Pierce, J. R., Kulmala, M., and Riipinen, I.: Semi-empirical parameterization of size-dependent atmospheric nanoparticle growth in continental environments, Atmos. Chem. Phys., 13, 7665–7682, https://doi.org/10.5194/acp-13-7665-2013, 2013.

Hellén, H., Praplan, A. P., Tykkä, T., Ylivinkka, I., Vakkari, V., Bäck, J., Petäjä, T., Kulmala, M., and Hakola, H.: Long-term measurements of volatile organic compounds highlight the importance of sesquiterpenes for the atmospheric chemistry of a boreal forest, Atmos. Chem. Phys., 18, 13 839–13 863, https://doi.org/10.5194/acp-18-13839-2018, 2018.

Hou, D., Zong, D., Lindberg, C. S., Kraft, M., and You, X.: On the coagulation efficiency of carbonaceous nanoparticles, J. Aerosol Sci., 140, 105 478, https://doi.org/https://doi.org/10.1016/j.jaerosci.2019.105478, 2020.

Kang, H. G., Takeuchi, M., Ng, N. L., Pöschl, U., and Berkemeier, T.: Multiphase Chemistry and Phase State Explain Nonlinear Effects in the Formation and Evaporation of SOA from Mixed Monoterpene Precursors, ACS ES&T Air, https://doi.org/10.1021/acsestair.5c00438, 2026.

Kenseth, C. M., Hafeman, N. J., Rezgui, S. P., Chen, J., Huang, Y., Dalleska, N. F., Kjaergaard, H. G., Stoltz, B. M., Seinfeld, J. H., and Wennberg, P. O.: Particle-phase accretion forms dimer esters in pinene secondary organic aerosol, Science, 382, 787–792, https://doi.org/10.1126/science.adi0857, 2023.

Kiland, K. J., Maclean, A. M., Kamal, S., and Bertram, A. K.: Diffusion of Organic Molecules as a Function of Temperature in a Sucrose Matrix (a Proxy for Secondary Organic Aerosol), J. Phys. Chem. Lett., 10, 5902–5908, https://doi.org/10.1021/acs.jpclett.9b02182, 2019.

Kirkby, J., Curtius, J., Almeida, J., Dunne, E., Duplissy, J., Ehrhart, S., Franchin, A., Gagné, S., Ickes, L., Kürten, A., Kupc, A., Metzger, A., Riccobono, F., Rondo, L., Schobesberger, S., Tsagkogeorgas, G., Wimmer, D., Amorim, A., Bianchi, F., Breitenlechner, M., David, A., Dommen, J., Downard, A., Ehn, M., Flagan, R. C., Haider, S., Hansel, A., Hauser, D., Jud, W., Junninen, H., Kreissl, F., Kvashin, A., Laaksonen, A., Lehtipalo, K., Lima, J., Lovejoy, E. R., Makhmutov, V., Mathot, S., Mikkilä, J., Minginette, P., Mogo, S., Nieminen, T., Onnela, A., Pereira, P., Petäjä, T., Schnitzhofer, R., Seinfeld, J. H., Sipilä, M., Stozhkov, Y., Stratmann, F., Tomé, A., Vanhanen, J., Viisanen, Y., Vrtala, A., Wagner, P. E., Walther, H., Weingartner, E., Wex, H., Winkler, P. M., Carslaw, K. S., Worsnop, D. R., Baltensperger, U., and Kulmala, M.: Role of sulphuric acid, ammonia and galactic cosmic rays in atmospheric aerosol nucleation, Nature, 476, 429–433, https://doi.org/10.1038/nature10343, 2011.

Knopf, D. A., Ammann, M., Berkemeier, T., Pöschl, U., and Shiraiwa, M.: Desorption lifetimes and activation energies influencing gas–surface interactions and multiphase chemical kinetics, Atmos. Chem. Phys., 24, 3445–3528, https://doi.org/10.5194/acp-24-3445-2024, 2024.

Koop, T., Bookhold, J., Shiraiwa, M., and Pöschl, U.: Glass transition and phase state of organic compounds: dependency on molecular properties and implications for secondary organic aerosols in the atmosphere, Phys. Chem. Chem. Phys., 13, 19 238, https://doi.org/10.1039/c1cp22617g, 2011.

Kulmala, M., Kontkanen, J., Junninen, H., Lehtipalo, K., Manninen, H. E., Nieminen, T., Petäjä, T., Sipilä, M., Schobesberger, S., Rantala, P., Franchin, A., Jokinen, T., Järvinen, E., Äijälä, M., Kangasluoma, J., Hakala, J., Aalto, P. P., Paasonen, P., Mikkilä, J., Vanhanen, J., Aalto, J., Hakola, H., Makkonen, U., Ruuskanen, T., Mauldin, R. L., Duplissy, J., Vehkamäki, H., Bäck, J., Kortelainen, A., Riipinen, I., Kurtén, T., Johnston, M. V., Smith, J. N., Ehn, M., Mentel, T. F., Lehtinen, K. E. J., Laaksonen, A., Kerminen, V.-M., and Worsnop, D. R.: Direct Observations of Atmospheric Aerosol Nucleation, Science, 339, 943–946, https://doi.org/10.1126/science.1227385, 2013.

Lehtipalo, K., Leppä, J., Kontkanen, J., Kangasluoma, J., Franchin, A., Wimnner, D., Schobesberger, S., Junninen, H., Petäjä, T., Sipilä, M., Mikkilä, J., Vanhanen, J., Worsnop, D., and Kulmala, M.: Methods for determining particle size distribution and growth rates between 1 and 3 nm using the Particle Size Magnifier, Boreal Environ. Res., 19, 215–236, 2014.

Li, Y., Pöschl, U., and Shiraiwa, M.: Molecular corridors and parameterizations of volatility in the chemical evolution of organic aerosols, Atmos. Chem. Phys., 16, 3327–3344, https://doi.org/10.5194/acp-16-3327-2016, 2016.

Li, Y., Day, D. A., Stark, H., Jimenez, J. L., and Shiraiwa, M.: Predictions of the glass transition temperature and viscosity of organic aerosols from volatility distributions, Atmos. Chem. Phys., 20, 8103–8122, https://doi.org/10.5194/acp-20-8103-2020, 2020.

Maben, H. K. and Ziemann, P. J.: Kinetics of oligomer-forming reactions involving the major functional groups present in atmospheric secondary organic aerosol particles, Environ. Sci.: Processes Impacts, 25, 214–228, https://doi.org/10.1039/D2EM00124A, 2023.

Mahant, S., Snider, J. R., Petters, S. S., and Petters, M. D.: Effect of Aerosol Size on Glass Transition Temperature, J. Phys. Chem. Lett., 15, 7509–7515, https://doi.org/10.1021/acs.jpclett.4c01415, 2024.

McNeill, V. F., Loerting, T., Geiger, F. M., Trout, B. L., and Molina, M. J.: Hydrogen chloride-induced surface disordering on ice, P. Natl. Acad. Sci. USA, 103, 9422–9427, https://doi.org/10.1073/pnas.0603494103, 2006.

Mehra, A., Krechmer, J. E., Lambe, A., Sarkar, C., Williams, L., Khalaj, F., Guenther, A., Jayne, J., Coe, H., Worsnop, D., Faiola, C., and Canagaratna, M.: Oligomer and highly oxygenated organic molecule formation from oxidation of oxygenated monoterpenes emitted by California sage plants, Atmos. Chem. Phys., 20, 10 953–10 965, https://doi.org/10.5194/acp-20-10953-2020, 2020.

Mikhailov, E., Vlasenko, S., Rose, D., and Pöschl, U.: Mass-based hygroscopicity parameter interaction model and measurement of atmospheric aerosol water uptake, Atmos. Chem. Phys., 13, 717–740, https://doi.org/10.5194/acp-13-717-2013, 2013.

Mishra, A., Kilchhofer, K., Iezzi, L., Pöschl, U., Alpert, P. A., Ammann, M., and Berkemeier, T.: Photochemical Degradation of Iron Citrate in Anoxic Viscous Films Enhanced by Redox Cascades, ACS Earth Space Chem., 9, 689–698, https://doi.org/10.1021/acsearthspacechem.4c00364, 2025.

Nguyen, K., Schervish, M., Lakey, P. S. J., Smith, J. N., and Shiraiwa, M.: Impact of particle phase state on the competition between condensation and coagulation, Environ. Sci.: Atmos., 6, 152–165, https://doi.org/10.1039/d5ea00069f, 2026.

Nieminen, T., Lehtinen, K. E. J., and Kulmala, M.: Sub-10 nm particle growth by vapor condensation – effects of vapor molecule size and particle thermal speed, Atmos. Chem. Phys., 10, 9773–9779, https://doi.org/10.5194/acp-10-9773-2010, 2010.

Pankow, J. F.: An absorption model of the gas/aerosol partitioning involved in the formation of secondary organic aerosol, Atmos. Environ., 28, 189–193, https://doi.org/10.1016/1352-2310(94)90094-9, 1994.

Petters, M. D. and Kreidenweis, S. M.: A single parameter representation of hygroscopic growth and cloud condensation nucleus activity, Atmos. Chem. Phys., 7, 1961–1971, https://doi.org/10.5194/acp-7-1961-2007, 2007.

Pöschl, U., Rudich, Y., and Ammann, M.: Kinetic model framework for aerosol and cloud surface chemistry and gas-particle interactions ndash; Part 1: General equations, parameters, and terminology, Atmos. Chem. Phys., 7, 5989–6023, https://doi.org/10.5194/acp-7-5989-2007, 2007.

Schervish, M. and Donahue, N. M.: Peroxy radical chemistry and the volatility basis set, Atmos. Chem. Phys., 20, 1183–1199, https://doi.org/10.5194/acp-20-1183-2020, 2020.

Seinfeld, J. H. and Pandis, S. N.: Atmospheric chemistry and physics: from air pollution to climate change, John Wiley & Sons, 2016.

Shiraiwa, M., Pfrang, C., Koop, T., and Pöschl, U.: Kinetic multi-layer model of gas-particle interactions in aerosols and clouds (KM-GAP): linking condensation, evaporation and chemical reactions of organics, oxidants and water, Atmos. Chem. Phys., 12, 2777–2794, https://doi.org/10.5194/acp-12-2777-2012, 2012.

Shiraiwa, M., Berkemeier, T., Schilling-Fahnestock, K. A., Seinfeld, J. H., and Pöschl, U.: Molecular corridors and kinetic regimes in the multiphase chemical evolution of secondary organic aerosol, Atmos. Chem. Phys., 14, 8323–8341, https://doi.org/10.5194/acp-14-8323-2014, 2014.

Shiraiwa, M., Li, Y., Tsimpidi, A. P., Karydis, V. A., Berkemeier, T., Pandis, S. N., Lelieveld, J., Koop, T., and Pöschl, U.: Global distribution of particle phase state in atmospheric secondary organic aerosols, Nat. Commun., 8, 15 002, https://doi.org/10.1038/ncomms15002, 2017.

Stevenson, J. D. and Wolynes, P. G.: On the surface of glasses, J. Chem. Phys., 129, 234 514, https://doi.org/10.1063/1.3041651, 2008.

Stolzenburg, D., Fischer, L., Vogel, A. L., Heinritzi, M., Schervish, M., Simon, M., Wagner, A. C., Dada, L., Ahonen, L. R., Amorim, A., Baccarini, A., Bauer, P. S., Baumgartner, B., Bergen, A., Bianchi, F., Breitenlechner, M., Brilke, S., Buenrostro Mazon, S., Chen, D., Dias, A., Draper, D. C., Duplissy, J., El Haddad, I., Finkenzeller, H., Frege, C., Fuchs, C., Garmash, O., Gordon, H., He, X., Helm, J., Hofbauer, V., Hoyle, C. R., Kim, C., Kirkby, J., Kontkanen, J., Kürten, A., Lampilahti, J., Lawler, M., Lehtipalo, K., Leiminger, M., Mai, H., Mathot, S., Mentler, B., Molteni, U., Nie, W., Nieminen, T., Nowak, J. B., Ojdanic, A., Onnela, A., Passananti, M., Petäjä, T., Quéléver, L. L. J., Rissanen, M. P., Sarnela, N., Schallhart, S., Tauber, C., Tomé, A., Wagner, R., Wang, M., Weitz, L., Wimmer, D., Xiao, M., Yan, C., Ye, P., Zha, Q., Baltensperger, U., Curtius, J., Dommen, J., Flagan, R. C., Kulmala, M., Smith, J. N., Worsnop, D. R., Hansel, A., Donahue, N. M., and Winkler, P. M.: Rapid growth of organic aerosol nanoparticles over a wide tropospheric temperature range, P. Natl. Acad. Sci. USA, 115, 9122–9127, https://doi.org/10.1073/pnas.1807604115, 2018.

Stolzenburg, D., Wang, M., Schervish, M., and Donahue, N. M.: Tutorial: Dynamic organic growth modeling with a volatility basis set, J. Aerosol Sci., 166, 106 063, https://doi.org/10.1016/j.jaerosci.2022.106063, 2022.

Stolzenburg, D., Cai, R., Blichner, S. M., Kontkanen, J., Zhou, P., Makkonen, R., Kerminen, V.-M., Kulmala, M., Riipinen, I., and Kangasluoma, J.: Atmospheric nanoparticle growth, Rev. Mod. Phys., 95, 045 002, https://doi.org/10.1103/RevModPhys.95.045002, 2023.

Stolzenburg, D., Sarnela, N., Bianchi, F., Cai, J., Cai, R., Cheng, Y., Dada, L., Donahue, N. M., Grothe, H., Holm, S., Kerminen, V.-M., Lehtipalo, K., Petäjä, T., Sulo, J., Winkler, P. M., Yan, C., Kangasluoma, J., and Kulmala, M.: Incomplete mass closure in atmospheric nanoparticle growth, npj Clim. Atmos. Sci., 8, https://doi.org/10.1038/s41612-025-00893-5, 2025.

Tian, H., Xu, Q., Zhang, H., Priestley, R. D., and Zuo, B.: Surface dynamics of glasses, Appl. Phys. Rev., 9, 011 316, https://doi.org/10.1063/5.0083726, 2022.

Tröstl, J., Chuang, W. K., Gordon, H., Heinritzi, M., Yan, C., Molteni, U., Ahlm, L., Frege, C., Bianchi, F., Wagner, R., Simon, M., Lehtipalo, K., Williamson, C., Craven, J. S., Duplissy, J., Adamov, A., Almeida, J., Bernhammer, A.-K., Breitenlechner, M., Brilke, S., Dias, A., Ehrhart, S., Flagan, R. C., Franchin, A., Fuchs, C., Guida, R., Gysel, M., Hansel, A., Hoyle, C. R., Jokinen, T., Junninen, H., Kangasluoma, J., Keskinen, H., Kim, J., Krapf, M., Kürten, A., Laaksonen, A., Lawler, M., Leiminger, M., Mathot, S., Möhler, O., Nieminen, T., Onnela, A., Petäjä, T., Piel, F. M., Miettinen, P., Rissanen, M. P., Rondo, L., Sarnela, N., Schobesberger, S., Sengupta, K., Sipilä, M., Smith,

J. N., Steiner, G., Tomè, A., Virtanen, A., Wagner, A. C., Weingartner, E., Wimmer, D., Winkler, P. M., Ye, P., Carslaw, K. S., Curtius, J., Dommen, J., Kirkby, J., Kulmala, M., Riipinen, I., Worsnop, D. R., Donahue, N. M., and Baltensperger, U.: The role of low-volatility organic compounds in initial particle growth in the atmosphere, Nature, 533, 527–531, https://doi.org/10.1038/nature18271, 2016.

Vignes, A.: Diffusion in Binary Solutions. Variation of Diffusion Coefficient with Composition, Ind. Eng. Chem. Fundam., 5, 189–199, https://doi.org/10.1021/i160018a007, 1966.

Virtanen, A., Joutsensaari, J., Koop, T., Kannosto, J., Yli-Pirilä, P., Leskinen, J., Mäkelä, J. M., Holopainen, J. K., Pöschl, U., Kulmala, M., Worsnop, D. R., and Laaksonen, A.: An amorphous solid state of biogenic secondary organic aerosol particles, Nature, 467, 824–827, https://doi.org/10.1038/nature09455, 2010.

Virtanen, A., Kannosto, J., Kuuluvainen, H., Arffman, A., Joutsensaari, J., Saukko, E., Hao, L., Yli-Pirilä, P., Tiitta, P., Holopainen, J. K., Keskinen, J., Worsnop, D. R., Smith, J. N., and Laaksonen, A.: Bounce behavior of freshly nucleated biogenic secondary organic aerosol particles, Atmos. Chem. Phys., 11, 8759–8766, https://doi.org/10.5194/acp-11-8759-2011, 2011.